

Exploring the Singlino-dominated Thermal Neutralino Dark Matter in the Z_3 invariant NMSSM

Amit Adhikary¹ Rahool Kumar Barman² Biplob Bhattacharjee³ Amandip De³ Rohini M. Godbole³

¹*Aix Marseille Univ., Université de Toulon, CNRS, CPT, IPhU, Marseille, France*

²*Kavli IPMU (WPI), UTIAS, The University of Tokyo, Kashiwa, Chiba 277-8583, Japan*

³*Centre for High Energy Physics, Indian Institute of Science, Bangalore 560012, India*

E-mail: amit.adhikary@cpt.univ-mrs.fr, rahool.barman@ipmu.jp,
biplob@iisc.ac.in, rohini@iisc.ac.in, amandipde@iisc.ac.in

ABSTRACT: We examine the parameter space of the Next to Minimal Supersymmetric Standard Model (NMSSM) with Singlino-dominated neutralino $\tilde{\chi}_1^0$ as the lightest supersymmetric particle (LSP). Our study focuses on identifying the regions within this parameter space that produce a thermal relic abundance of $\tilde{\chi}_1^0$ smaller than the observed cold dark matter relic density while remaining consistent with constraints from LEP measurements, low-energy experiments, Higgs measurements, LHC data, and dark matter direct detection experiments. We identify the dominant annihilation modes of the LSP neutralino across varying LSP mass ranges $\sim \mathcal{O}(1) - \mathcal{O}(10^3)$ GeV. Furthermore, we conduct a benchmark study to assess the production rates of triple-boson final states emerging from direct electroweakino pair production at the LHC. Drawing insights from these findings, we perform a detailed collider analysis to explore the future potential of probing the triple-boson final states involving a light Higgs boson at the high-luminosity LHC (HL-LHC).

Contents

1	Introduction	1
2	The NMSSM framework	3
3	Parameter space scan and constraints	6
4	Annihilation processes with Singlino LSP	12
5	Benchmark Scenario	14
6	Direct Electroweakino searches in the ZWH_1 channel	16
7	Conclusion	21
A	Indirect detection	23
B	Summarising the cross sections and generator level cuts for the SM backgrounds	23

1 Introduction

The nature of Dark Matter (DM) remains a central mystery in contemporary particle physics, particularly within the realm of Beyond Standard Model (BSM) physics. Unveiling the properties of DM candidates is a key objective, driving extensive experimental efforts that employ direct, indirect [1, 2] and collider searches [3, 4]. Among the proposed DM candidates, a Weakly Interacting Massive Particle (WIMP), an example of non-baryonic Cold Dark Matter (CDM) candidate interacting via electroweak coupling with a mass around the electroweak scale, can naturally predict a relic density that aligns very closely to the measured value of $\Omega h^2 = 0.120 \pm 0.001$ in the PLACK experiment at 68% C.L. [5]. WIMPs are one of the favourable DM candidates since they can be produced at the thermal equilibrium conditions prevailing in this surprising agreement, referred to as the ‘WIMP miracle’ [6–8]. The non-relativistic nature and weak interactions of WIMPs lead to two primary categories for DM-nucleon scattering: spin-independent (SI) and spin-dependent (SD). The recent LUX-ZEPLIN (LZ) experiment has reported the most stringent limit of DM-nucleon SI elastic scattering cross-section (σ_{SI}) at $9.2 \times 10^{-48} \text{ cm}^2$ at the 90% C.L. corresponding to DM particle mass at 36 GeV [9]. While the SD WIMP-nuclear cross-section has the minimum limit for 30 and 25 GeV WIMPs at 1.49×10^{-42} and $3.2 \times 10^{-41} \text{ cm}^2$ from LZ and PICO-60 C_3F_8 experiments for SD WIMP-neutron (σ_{SD_n}) and SD WIMP-proton (σ_{SD_p}) cross-sections [9, 10]. LZ for 1000 live day run has projected an increase by around an order of magnitude in these cross-sections [11].

These strong limits on SI and SD DM-nucleon scattering indicate the feeble nature of the DM and nucleon interactions, which poses significant experimental challenges [12]. This necessitates exploring alternative avenues for DM detection, such as searching for missing energy signatures in experiments at the LHC.

The absence of any DM candidate in the SM strongly suggests looking for possible BSM scenarios to explain the observed dark matter. A very well-motivated model, Supersymmetry, can provide a possible dark matter candidate, the lightest neutralino, within R-parity conserved scenario [13, 14]. The neutralino sector in Minimal Supersymmetric Standard Model (MSSM) involves the mixing of Bino (\tilde{B}), Wino (\tilde{W}), and neutral Higgsinos (\tilde{H}_u and \tilde{H}_d), to produce four neutralinos. The lightest neutralino ($\tilde{\chi}_1^0$), denoted as the lightest supersymmetric particle (LSP), a Majorana spin 1/2 particle, is usually the most popular candidate for DM. In phenomenological MSSM (pMSSM), LSP mass must exceed 34 GeV to avoid over-abundant relic density [15–19]. For single-component thermal DM in the general MSSM, Higgsinos are favoured to be massive ($\gtrsim 1$ TeV) to achieve the correct DM abundance [20–22]. This avoids an overly large annihilation rate unless stops are very heavy [23, 24] or the Higgsino mass parameter (μ) is negative [25]. In the low-mass limit ($\lesssim 1$ TeV), a Bino-dominated LSP with significant co-annihilation from Wino-like neutralinos is preferred to match the observed relic density. The parameter μ receives constraints from both the theory and experimental front. Moreover, a large value of Higgsino mass parameter μ far above the value of M_Z is disfavored in the MSSM since it is not *natural* and can introduce a “little fine-tune problem” [26–28]. This can be evaded in a model featuring a singlet extension of the MSSM, the Next-to-Minimal Supersymmetric Standard Model (NMSSM) [29–31], which introduces a singlet Higgs field in addition to two Higgs doublets of the MSSM. In NMSSM, the μ parameter is generated dynamically when the singlet field develops a vacuum expectation value (*vev*) v_S , with Z_3 symmetry in the NMSSM, $\mu = \lambda v_S$ at the electroweak scale.

The NMSSM introduces an extended Higgs sector with seven Higgs bosons: three CP-even, two CP-odd neutrals, and two charged ones. Interestingly, this allows for a light singlet-dominated scalar (H_1) or singlet-dominated pseudoscalar Higgs (A_1) potentially lighter than the SM-like Higgs (H_{SM}) satisfying the collider constraints [32–37]. Likewise, the Singlino, fermionic superpartner of singlet field, expands the neutralino sector to five states, where the lightest of these neutralinos remains a viable candidate for DM [38–46]. The singlet-like light scalars (H_1/A_1) are important to our current study, where along with it, a Singlino-dominated LSP containing critical amount of Higgsino admixture for moderate values of μ [47–50] can provide under-abundant relic. In exceedingly low mass regions, this scenario offers new annihilation funnels via light Higgs along with correct Singlino admixture in LSP to satisfy the limits of DM DD, which was not possible in MSSM [48, 49]. In the relatively high mass regions, the usual co-annihilation mechanism dominates where Higgsino admixture allows the LSP to efficiently annihilate in the early universe and, in turn, increase the interaction strength of LSP, making it more detectable in DM DD experiments. Moreover, considering a slight Bino content in the LSP for suitably small M_1 , could provide us with a viable Singlino-dominated DM candidate, which allows funnels featuring SM Higgs boson, Z-boson and even the light singlet-like Higgs [35, 51]. Given a low-mass Singlino-like DM candidate, we primarily aim to study if this type of scenario is still compatible with the DM DD and collider searches. Then, look for possible interesting channels involving decays to Singlino-like LSP and their sensitivity of detection at high luminosity LHC in the framework of NMSSM.

Usually, the interesting channels involve cascade decays of MSSM-like NLSPs to Singlino-like LSP where the decays of heavier neutralinos and charginos proceed via the emission of on/off shell gauge and Higgs bosons $Z/W^\pm/H_{SM}/H_1/A_1$ when the sparticles in the model are heavy, and the electroweakinos do not form a compressed spectrum. Particularly, the condition $m_{LSP} < M_1 < \mu$ in NMSSM facilitate typical decays $\tilde{\chi}_1^\pm \rightarrow \tilde{\chi}_1^0/\tilde{\chi}_2^0 W^\pm, \tilde{\chi}_i^0 \rightarrow Z/H_{SM}/H_1/A_1 \tilde{\chi}_1^0$. In this work, we only include the triple-boson channels [52–55] from the Higgsino-like chargino-neutralino production, which is otherwise not native to MSSM. These triple-bosons are usually detected via their leptonic decays, leading to a signal final state consisting of \cancel{E}_T and leptons. Some specific consequences of such possibilities incorporate light singlet Higgs producing collimated decays to $b\bar{b}/\tau\tau/W^\pm W^\pm/\gamma\gamma$. We study one such possibility where H_1 decays to $b\bar{b}$ and appears as a single fatjet. A few studies have been performed at the LHC to search light scalar in decays $\tau\tau$ [56], $b\bar{b}$ [36, 57], $\gamma\gamma$ [41, 58, 59]. To summarize, we look for a signal final state consisting of a Higgs fatjet, leptons plus \cancel{E}_T and predict the sensitivity at HL-LHC.

The paper is organized as follows. In Sec. 2, we revisit the Higgs and electroweakino sectors in the NMSSM framework. We discuss the range of parameters for our scan, relevant collider and astrophysical constraints, and their impact on the parameter space of our interest in Sec. 3. We examine the different DM annihilation modes responsible for effective DM dilution in the early universe, through which consistency with relic density constraints is achieved in Sec. 4. In Sec. 5, we discuss the benchmark scenario adopted for analyzing the HL-LHC potential for direct electroweakino pair production in the triple boson + \cancel{E}_T final state. The details of the collider search are presented in Sec. 6. We conclude in Sec. 7.

2 The NMSSM framework

We consider the Z_3 -invariant NMSSM with the superpotential [30],

$$W_{\text{NMSSM}} = W_{\text{MSSM}}|_{\mu=0} + \lambda \hat{S} \hat{H}_u \cdot \hat{H}_d + \frac{\kappa}{3} \hat{S}^3, \quad (2.1)$$

where, $W_{\text{MSSM}}|_{\mu=0}$ denotes the MSSM superpotential without the μ -term, \hat{H}_u and \hat{H}_d are the two doublet Higgs superfields similar to that in MSSM, and \hat{S} is a gauge singlet Higgs superfield. The dimensionless parameters, “ λ ” and “ κ ”, control the mixing between the doublet and singlet Higgs superfields and self-coupling of the singlet superfield, respectively. The superpotential in Eq. (2.1) provides a solution to the MSSM μ -problem by generating an effective μ -term, $\mu = \lambda v_S$, when, \hat{S} develops a vacuum expectation value v_S .

The Higgs scalar potential V_{Higgs} receives contributions from the soft SUSY breaking terms V_{soft} [30],

$$V_{\text{soft}} = m_{H_u}^2 |H_u|^2 + m_{H_d}^2 |H_d|^2 + m_S^2 |S|^2 + \left(\lambda A_\lambda S H_u \cdot H_d + \frac{1}{3} \kappa A_\kappa S^3 + \text{h.c.} \right), \quad (2.2)$$

where, m_{H_u} , m_{H_d} , m_S are the soft breaking Higgs masses and A_λ , A_κ are the trilinear couplings with dimensions of mass. The full scalar Higgs potential is obtained by combining V_{soft} with the

F and D terms, $V_{Higgs} = V_{soft} + V_D + V_F$, with,

$$\begin{aligned} V_F &= |\lambda H_u \cdot H_d + \kappa S^2|^2 + \lambda^2 |S|^2 \left(H_u^\dagger H_u + H_d^\dagger H_d \right), \text{ and} \\ V_D &= \frac{g_1^2 + g_2^2}{8} \left(H_u^\dagger H_u - H_d^\dagger H_d \right)^2 + \frac{g_2^2}{2} |H_d^\dagger H_u|^2. \end{aligned} \quad (2.3)$$

In Eq. (2.3), g_1 and g_2 are the SM $U(1)_Y$ and $SU(2)_L$ gauge couplings, respectively. Expanding V_{Higgs} around the real neutral *vevs* v_d, v_u and v_S , we obtain the physical neutral Higgs fields $\{H_d^0, H_u^0, S\}$,

$$H_d^0 = v_d + \frac{H_{dR} + iH_{dI}}{\sqrt{2}}, \quad H_u^0 = v_u + \frac{H_{uR} + iH_{uI}}{\sqrt{2}}, \quad S = v_S + \frac{S_R + iS_I}{\sqrt{2}}, \quad (2.4)$$

where, the subscripts R and I indicate the CP-even and CP-odd states of $\{H_d^0, H_u^0, S\}$, respectively. In the basis $\{H_{dR}, H_{uR}, S_R\}$, the 3×3 symmetric mass-squared matrix \mathcal{M}_S^2 for the CP-even neutral Higgs states is given by [30],

$$\mathcal{M}_S^2 = \begin{pmatrix} g^2 v_d^2 + \mu(A_\lambda + \kappa v_S) \tan \beta & (2\lambda^2 - g^2) v_u v_d - \mu(A_\lambda + \kappa v_S) & \lambda(2\mu v_d - (A_\lambda + 2\kappa v_S) v_u) \\ \dots & g^2 v_u^2 + \mu(A_\lambda + \kappa v_S) / \tan \beta & \lambda(2\mu v_u - (A_\lambda + 2\kappa v_S) v_d) \\ \dots & \dots & \lambda A_\lambda \frac{v_u v_d}{v_S} + \kappa v_S (A_\kappa + 4\kappa v_S) \end{pmatrix}, \quad (2.5)$$

where $g^2 = (g_1^2 + g_2^2)/2$, $v_u = v \sin \beta$ and $v_d = v \cos \beta$ with $v^2 = v_u^2 + v_d^2 \approx (174 \text{ GeV})^2$, and $\tan \beta = v_u/v_d$. The CP-even Higgs mass eigenstates H_i ($i = 1, 2, 3$) can be obtained by diagonalizing \mathcal{M}_S^2 by the matrix S , such that

$$H_i = \sum_{j=1}^3 S_{ij} H_{jR}, \quad \text{with} \quad H_{jR} = \{H_{uR}, H_{dR}, S_R\}. \quad (2.6)$$

Assuming negligible mixing between the doublet and singlet components, the squared mass of the singlet-dominated CP-even state at the tree-level is given by the (3,3) element of \mathcal{M}_S^2 ,

$$m_{H_S}^2 \approx \mathcal{M}_{S33}^2 = \lambda A_\lambda \frac{v_u v_d}{v_S} + \kappa v_S (A_\kappa + 4\kappa v_S). \quad (2.7)$$

Under this assumption, one of the other two CP-even eigenstates must be consistent with the observed SM-like Higgs boson with a mass near 125 GeV, and the other one is a MSSM-like Higgs eigenstate with squared mass around

$$m_{H_3}^2 = 2\mu(A_\lambda + \kappa v_S) / \sin 2\beta \quad (2.8)$$

In this scenario, the CP-even Higgs bosons can be conveniently rotated to the basis $\{\hat{h}, \hat{H}, \hat{s}\}$ [60, 61], such that $\hat{h} = H_{dR} \cos \beta + H_{uR} \sin \beta$, $\hat{H} = H_{dR} \sin \beta - H_{uR} \cos \beta$ and $\hat{s} = S_R$, with \hat{h} and \hat{H} fields resembling the SM-like Higgs boson and the MSSM-like heavy Higgs bosons, respectively. The mass eigenstates in this basis can then be expressed as,

$$H_i = V_{h_i \hat{h}} \hat{h} + V_{h_i \hat{H}} \hat{H} + V_{h_i \hat{s}} \hat{s} \quad \text{where} \quad (i = 1, 2, 3) \quad (2.9)$$

where V represents the 3×3 unitary matrix that diagonalizes the mass-squared matrix of CP-even Higgs bosons in the rotated basis $\{\hat{h}, \hat{H}, \hat{s}\}$.

The mass of SM-like Higgs boson H_{SM} at the one-loop level can be written as [62],

$$m_{H_{SM}}^2 = m_Z^2 \cos^2 2\beta + \lambda^2 v^2 \sin^2 2\beta + \Delta_{mix} + \Delta_{rad.corr.} \quad (2.10)$$

Here, the second term implies that a large λ and low $\tan \beta$ is typically favorable to uplift $m_{H_{SM}}$ from $\sim m_Z$ and bring it closer to the observed mass of ~ 125 GeV at the tree-level, thus typically reducing the amount of radiative corrections required to generate the correct Higgs boson mass, when compared to MSSM. The third term in Eq. (2.10), Δ_{mix} , is the contribution arising from singlet-doublet mixing. In the limit where the mixing is not large, Δ_{mix} is given by [62],

$$\Delta_{mix} \simeq \frac{4\lambda^2 v_S^2 v^2 (\lambda - \kappa \sin 2\beta)^2}{(\overline{M}_h^2 - M_{SS}^2)}, \quad (2.11)$$

where, $\overline{M}_h^2 = m_{H_{SM}}^2$ (given by Eq. (2.10)) for $\Delta_{mix} \sim 0$, and $M_{SS}^2 \simeq \kappa v_S (A_\kappa + 4\kappa v_S)$ is the squared mass of CP-even singlet-like Higgs assuming a heavy singlet, $\kappa v_S \gg A_\kappa, A_\lambda$ (see Eq. (2.7)). The contribution from this term can be positive or negative depending on the mass difference $\overline{M}_h^2 - M_{SS}^2$.

In the decoupling limit, $\lambda, \kappa \rightarrow 0$, the radiative corrections to $m_{H_{SM}}$, $\Delta_{rad.corr.}$, become crucial to obtain the correct mass for the SM-like Higgs boson. The dominant radiative contributions at one-loop from the top/stop loops are given by,

$$\Delta_{rad.corr.}^{1-loop} \simeq \frac{3m_t^4}{4\pi^2 v^2 \sin^2 \beta} \left[\ln \frac{M_S^2}{m_t^2} + \frac{X_t^2}{M_S^2} \left(1 - \frac{X_t^2}{12M_S^2} \right) \right], \quad (2.12)$$

where, m_t denotes top quark mass, $M_S = \sqrt{m_{\tilde{t}_1} m_{\tilde{t}_2}}$ with $m_{\tilde{t}_1, \tilde{t}_2}$ stands for mass ordered stop squarks and $|X_t| = A_t - \mu \cot \beta$ is stop mixing parameter with A_t being the soft supersymmetry-breaking stop trilinear coupling.

Similar to Eq. (2.5), the mass squared matrix $\mathcal{M}'_{\mathcal{P}}{}^2$ for the CP-odd states (H_{dI}, H_{uI}, S_I) from Eq. (2.4) can be defined as [30],

$$\mathcal{M}'_{\mathcal{P}}{}^2 = \begin{pmatrix} \mu(A_\lambda + \kappa v_S) \tan \beta & \mu(A_\lambda + \kappa v_S) & \lambda v_u(A_\lambda - 2\kappa v_S) \\ \dots & \mu(A_\lambda + \kappa v_S)/\tan \beta & \lambda v_d(A_\lambda - 2\kappa v_S) \\ \dots & \dots & \lambda(A_\lambda + 4\kappa v_S) \frac{v_u v_d}{v_S} - 3\kappa A_\kappa v_S \end{pmatrix}. \quad (2.13)$$

Without any loss of generality, the mass matrix $\mathcal{M}'_{\mathcal{P}}{}^2$ can be rotated to a new basis, $\{H_{dI}, H_{uI}, S_I\} \rightarrow \{A, G, S_I\}$,

$$\begin{pmatrix} H_{dI} \\ H_{uI} \\ S_I \end{pmatrix} = \begin{pmatrix} \sin \beta & -\cos \beta & 0 \\ \cos \beta & \sin \beta & 0 \\ 0 & 0 & 1 \end{pmatrix} \begin{pmatrix} A \\ G \\ S_I \end{pmatrix}. \quad (2.14)$$

Dropping the Goldstone mode G , the remaining 2×2 mass squared matrix for CP-odd states in the basis of $\{A, S_I\}$ can be expressed as,

$$\mathcal{M}_{\mathcal{P}}{}^2 = \begin{pmatrix} m_A^2 & \lambda(A_\lambda - 2\kappa v_S)v \\ \lambda(A_\lambda - 2\kappa v_S)v & \lambda(A_\lambda + 4\kappa v_S) \frac{v_u v_d}{v_S} - 3\kappa A_\kappa v_S \end{pmatrix}, \quad (2.15)$$

with $m_A^2 = 2\mu(A_\lambda + \kappa v_S)/\sin 2\beta$, which represents the squared mass of the doublet-like CP-odd scalar, A , similar to that in the MSSM. Likewise, the squared mass of the singlet-like CP-odd scalar A_s , assuming negligible singlet-doublet mixing, is represented by the $\{2, 2\}$ element in $\mathcal{M}_{\mathcal{P}}{}^2$.

Overall, the scalar sector is characterized by six parameters:

$$\lambda, \kappa, A_\lambda, A_\kappa, \mu, \tan \beta, \quad (2.16)$$

as indicated by Eqs.(2.7), (2.10) and (2.15).

The electroweakino sector of NMSSM consists of 5 neutralinos and 2 charginos. The 5×5 symmetric neutralino mass matrix $\mathcal{M}_{\tilde{N}}$ in the basis of $\{\tilde{B}$: Bino, \tilde{W}_3^0 : Wino, $\tilde{H}_d^0, \tilde{H}_u^0$: Higgsinos, and \tilde{S} : Singlino $\}$ is given by,

$$\mathcal{M}_{\tilde{N}} = \begin{pmatrix} M_1 & 0 & -\frac{g_1 v_d}{\sqrt{2}} & \frac{g_1 v_u}{\sqrt{2}} & 0 \\ \dots & M_2 & \frac{g_2 v_d}{\sqrt{2}} & -\frac{g_2 v_u}{\sqrt{2}} & 0 \\ \dots & \dots & 0 & -\mu_{eff} & -\lambda v_u \\ \dots & \dots & \dots & 0 & -\lambda v_d \\ \dots & \dots & \dots & \dots & -2\kappa v_S \end{pmatrix} \quad (2.17)$$

where M_1 and M_2 are the Bino and Wino mass parameters. The neutralino mass eigenstates $m_{\tilde{\chi}_i^0}$ ($i=1, \dots, 5$) can be obtained by diagonalizing $\mathcal{M}_{\tilde{N}}$ through an orthogonal real matrix N ,

$$\tilde{\chi}_i^0 = N_{i1}\tilde{B} + N_{i2}\tilde{W}_3^0 + N_{i3}\tilde{H}_d^0 + N_{i4}\tilde{H}_u^0 + N_{i5}\tilde{S}; \quad (2.18)$$

where the neutralino masses are not necessarily positive but ordered according to their absolute value.

The remaining components in the electroweakino sector are the two charginos ($\tilde{\chi}_i^\pm$ ($i = 1, 2$)), which are formed through mixing between the charged Winos and Higgsinos. In the basis $\psi^+ = (-i\tilde{W}^+, \tilde{H}_u^+)$ and $\psi^- = (-i\tilde{W}^-, \tilde{H}_d^-)$, the 2×2 asymmetric chargino mass matrix can be written as [30],

$$\mathcal{M}_C = \begin{pmatrix} M_2 & g_2 v_u \\ g_2 v_d & \mu \end{pmatrix} \quad (2.19)$$

The diagonalization of \mathcal{M}_C is accomplished by two different rotations, ψ^+ and ψ^- denoted by two unitary matrix U and V , respectively:

$$U^* \mathcal{M}_C V^\dagger = \text{diag}(m_{\tilde{\chi}_1^\pm}, m_{\tilde{\chi}_2^\pm}); \quad \text{with } m_{\tilde{\chi}_1^\pm} < m_{\tilde{\chi}_2^\pm}. \quad (2.20)$$

Overall, the electroweakino sector at the tree-level is characterized by six input parameters:

$$M_1, M_2, \mu, \tan \beta, \lambda, \kappa. \quad (2.21)$$

In the R-parity conserved NMSSM, the lightest neutralino $\tilde{\chi}_1^0$ emerges as a potential candidate for dark matter. As indicated by Eq. (2.18), LSP $\tilde{\chi}_1^0$ can be either \tilde{B} , \tilde{W} , \tilde{H} or \tilde{S} -like, or a hybrid of these states. While the pure \tilde{B} and \tilde{S} -like $\tilde{\chi}_1^0$ results in a correct relic abundance through resonant annihilation or co-annihilation, Winos or Higgsinos up to masses of 2.8 TeV tends to produce the correct relic density through self-annihilation.

3 Parameter space scan and constraints

In this work, we concentrate on the region of Z_3 -invariant NMSSM parameter space that leads to Singlino-dominated LSP, $\tilde{\chi}_1^0$, with under-abundant relic density. In the $\lambda \rightarrow 0$ limit, the singlet

superfield decouples from the MSSM Higgs superfields, as indicated by Eq. (2.1). In this decoupled regime, the mass of the Singlino-like neutralino at the tree-level is approximately $\sim 2\kappa v_S$. Given the effective Higgsino mass parameter $\mu = \lambda v_S$, and our region of interest being the parameter space with a Singlino-dominated LSP $\tilde{\chi}_1^0$, we require $2\kappa v_S \lesssim \lambda v_S$. Accordingly, we impose $|\kappa/\lambda| < 0.5$ in our scans to ensure Singlino dominance in the LSP $\tilde{\chi}_1^0$. Values of $\kappa, \lambda < 10^{-3}$ are avoided as to ensure beyond-the-MSSM scenario. It is also worth noting that perturbativity of the theory up to the GUT scale requires both $\lambda, \kappa < 0.7$. Based on initial results from our scan, we restrict λ to less than 0.4 to increase the likelihood of generating points with Singlino-dominated LSP. Our scan considers a wide range for the Bino, Wino and Higgsino mass parameters: $70 \text{ GeV} < M_1 < 2 \text{ TeV}$, $200 \text{ GeV} < M_2 < 3 \text{ TeV}$ and $100 \text{ GeV} < \mu < 900 \text{ GeV}$, respectively. M_2 is varied from a higher minimum value due to more stricter constraints on Winos. This choice of M_1 , M_2 , and μ allows the study of a diverse electroweakino sector within the NMSSM, involving various admixtures from Bino, Wino, and Higgsinos in the Singlino-dominated LSP. A small value of A_κ tends to favor a singlet-dominated light Higgs bosons, which could be crucial for resonant DM annihilation at low LSP masses, $m_{\tilde{\chi}_1^0} \lesssim m_Z/2$. Therefore, we vary it in the $[0-1000] \text{ GeV}$ range. Other key input parameters required to characterize the Higgs and electroweakino sectors at the tree level are A_κ and $\tan\beta$, which have been varied in the $[-10, 10^4] \text{ GeV}$ and $[1, 40]$ ranges, respectively. The third-generation squark mass parameters MQ_3, MU_3, MD_3 are varied in the range $[500-10^4] \text{ GeV}$, while the third-generation slepton mass parameters are fixed at 3 TeV . The second-generation squark and slepton mass parameters are also fixed at 3 TeV . Lastly, we vary the stop trilinear coupling A_t in the range $[-10, 10] \text{ TeV}$, while the bottom and stau trilinear couplings are fixed at $A_b = A_\tau = 2 \text{ TeV}$.

We perform a random scan over the parameter space, considering the previously discussed scan range, utilizing the `NMSSMTools-v6.0.0` [63–65] package. The masses and relevant branching ratios of the Higgs bosons and the SUSY particles are computed using `NMSSMTools-v6.0.0` [63–65]. We use `MicrOmegas` [66–68] to compute the observables constrained by LEP, B -physics experiments, and DM measurements. We initially perform a flat random scan over 10^8 points. Roughly $10^{-4}\%$ of the scanned points pass the relevant collider and astrophysical constraints. The range of input parameters considered in the scan is summarized below:

$$\begin{aligned}
0.0001 < \lambda < 0.4, \quad \left| \frac{\kappa}{\lambda} \right| &\leq 0.5, \quad M_1 = (70, 2000) \text{ GeV}, \\
M_2 &= (200, 3000) \text{ GeV}, \quad M_3 = (2000, 5000) \text{ GeV}, \\
\mu &= (100, 900) \text{ GeV}, \quad \tan\beta = (1, 40), \\
A_\lambda &= (-10, 10000) \text{ GeV}, \quad |A_\kappa| = (0, 1000) \text{ GeV}, \\
A_t &= (-10000, 10000) \text{ GeV} \\
A_b &= A_\tau = 2000 \text{ GeV} \\
ML_3 &= ME_3 = 2000 \text{ GeV} \\
MQ_3 &= MU_3 = MD_3 = (0.5, 10) \text{ TeV}
\end{aligned} \tag{3.1}$$

Constraints from collider experiments

The NMSSM parameter space of our interest is constrained by various collider and astrophysical measurements. We first discuss the relevant collider constraints. Adhering to LEP measurements,

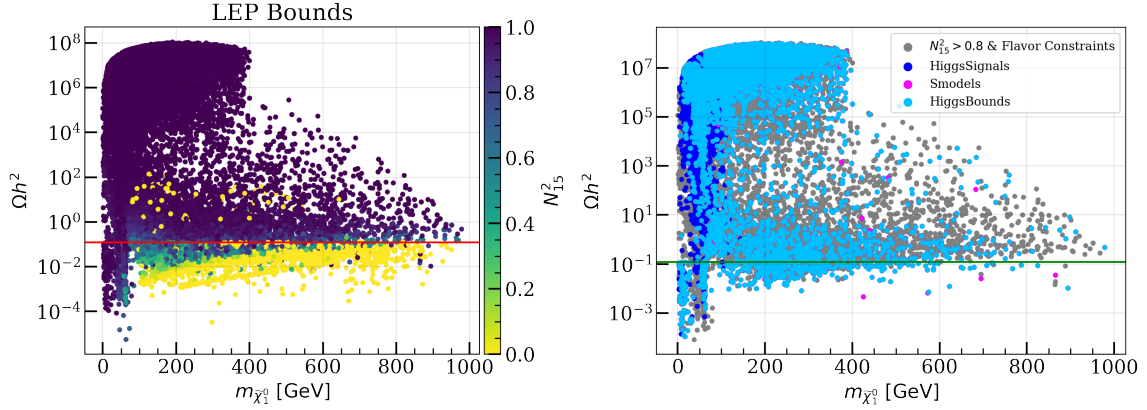


Figure 1: *Left:* Parameter points allowed by the theoretical constraints and LEP limits are shown in the $m_{\tilde{\chi}_1^0}$ - Ωh^2 plane. The color palette represents the Singlino admixture N_{15}^2 in the LSP $\tilde{\chi}_1^0$. *Right:* Parameter points allowed by the successive application of flavor constraints and the requirement of a Singlino-dominated $\tilde{\chi}_1^0$ ($N_{15}^2 > 0.8$) (shown in grey), Higgs signal-strength constraints imposed through `HiggsSignals-v2.6.2` [69, 70] (blue), bounds from electroweakino, gluino, squark, stop and sbottom searches at the LHC applied through `SModels-v2.3.2` [71, 72] (pink) and the limits from BSM Higgs searches at the LHC implemented via `HiggsBounds-v5.10.0` [69, 73–75] (skyblue), are shown in the same plane.

we require the mass of the charginos to be $M_{\tilde{\chi}_1^\pm} > 103.5$ GeV [76] and the production rate of the process $e^+e^- \rightarrow \tilde{\chi}_2^0\tilde{\chi}_1^0$ in the jets+ \cancel{E}_T final state with $|M_{\tilde{\chi}_2^0} - M_{\tilde{\chi}_1^0}| < 5$ GeV to be below ≤ 0.1 pb at 95% C.L. Limits from searches in the ZH_j and A_iH_j processes are imposed through `NMSSMTools-v6.0.0` [63–65]. In the left panel of Fig. 1, we display the parameter space in the $m_{\tilde{\chi}_1^0}$ - Ωh^2 plane, consistent with the LEP limits. The color axis represents the amount of Singlino admixture, N_{15}^2 in $\tilde{\chi}_1^0$. The imposed upper limit on the relic density $\Omega_{\tilde{\chi}_1^0} h^2 < 0.122$ is indicated as a solid red line in Fig. 1 (left). Furthermore, for these over-abundant points, it is typically observed that $|\kappa|/\lambda > 0.3$ in the higher $m_{\tilde{\chi}_1^0} \gtrsim 100$ region. Such points typically lead to an MSSM-like scenario with Higgsino-like dark matter. Notably, around 24% of points below $\Omega_{\tilde{\chi}_1^0} h^2 < 0.122$ are Singlino-dominated with $N_{15}^2 > 0.8$, which are the primary focus on this analysis.

The parameter space of interest is also constrained by flavor physics observables, especially through measurements of the rare decay of B -mesons. Updated constraints from flavor physics are also imposed from `NMSSMTools-v6.0.0` [63–65] in terms of $BR(b \rightarrow s\gamma)$, $BR(B_s \rightarrow \mu^+\mu^-)$, $BR(B^+ \rightarrow \tau^+\nu_\tau)$, $BR(B \rightarrow X_s\mu^+\mu^-)$. Additionally constraints from $\Upsilon(1s) \rightarrow H/A\gamma$, ΔM_s , ΔM_d , $\eta_b(1s)$ mass difference are imposed.

Among the three CP-even Higgs bosons, we require either H_1 or H_2 to be consistent with the properties of the observed SM-like Higgs boson H_{SM} . The mass of H_{SM} has been measured at 125.28 ± 0.14 GeV through combined measurements by the ATLAS and CMS collaborations at the LHC [77, 78]. To account for the theoretical uncertainties in the Higgs boson mass calculation [79], we adopt a conservative approach and require the mass of the Higgs boson consistent with H_{SM} to be within 122-128 GeV. Its couplings with $t\bar{t}$, $b\bar{b}$, $\tau^+\tau^-$, $\gamma\gamma$, W^+W^- , ZZ and gg are also required to be consistent with the signal strength measurements within 2σ uncertainty, imposed through the `HiggsSignals-v2.6.2` [69, 70] package. The heavier and/or lighter scalar and pseudoscalar

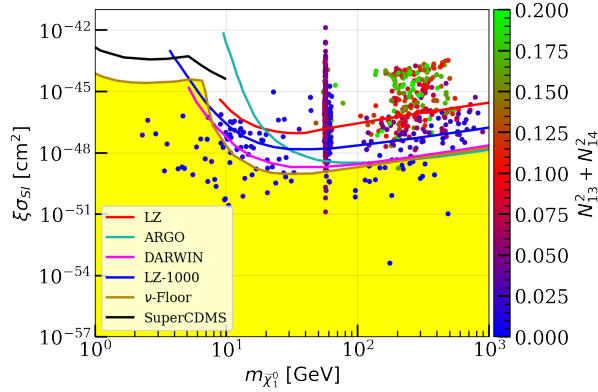


Figure 2: Parameter space points with a Singlino-dominated LSP, and allowed by searches at the LEP, rare B -meson decay, Higgs signal strength, and BSM Higgs, electroweakino and other particle searches at the LHC (sky-blue points from the right panel of Fig. 1) are shown in the $\xi\sigma_{SI} - m_{\tilde{\chi}_1^0}$ plane. The color palette represents the Higgsino fraction in the LSP. The red lines denote the current upper limit of σ_{SI} from the LZ results at 90% C.L [9]. Projected limits on σ_{SI} from future experiments, ARGO [81], DARWIN [82, 83], and LZ-1000 [11] are also presented.

Higgs bosons can be an admixture of doublet and singlet states and are primarily constrained by BSM Higgs searches at the LEP, Tevatron and the LHC. We impose these constraints using `HiggsBounds-v5.10.0` [69, 73–75]. Limits from the searches for supersymmetric particles at the LHC, especially electroweakinos, are implemented using `SModels-v2.3.2` [71, 72] interfaced with `NMSSMTools-v6.0.0` [63–65].

Constraints from relic density of dark matter and direct detection

As discussed previously, our main focus is the region of parameter space where the Singlino-dominated LSP $\tilde{\chi}_1^0$ serves as the thermal DM candidate. In this scenario, the Dark Matter relic abundance of $\tilde{\chi}_1^0$ is required to be within $\Omega_{\tilde{\chi}_1^0} h^2 < 0.122$, allowing a 2σ uncertainty around the best-fit of $\Omega_{DM}^{obs} h^2 = 0.120 \pm 0.001$ as measured by the PLANCK collaboration [5].

The parameter space points that survive the previously discussed constraints are further subjected to the most recent upper limits on the spin-independent DM-nucleon cross-sections σ_{SI} , from LZ [9]. We also impose the upper limits from SuperCDMS [80], which is sensitive in the lower m_{DM} regime, $100 \text{ MeV} \lesssim m_{DM} \lesssim 5 \text{ GeV}$. We rescale σ_{SI} with ξ , the ratio of the DM relic density predicted by the model to the observed upper limit on $\Omega_{DM}^{obs} h^2$ allowing 3σ uncertainty, $\xi = \Omega h^2 / 0.122$. In Fig. 2, we illustrate the parameter points allowed by the previously discussed constraints in the plane of $\xi\sigma_{SI}$ and $m_{\tilde{\chi}_1^0}$. Among them, approximately 70% of points are excluded by LZ SI limits. We also illustrate the projected sensitivity of ARGO [81], DARWIN [82, 83], and LZ-1000 [11], in probing σ_{SI} in the same plot. It is observed that a sizeable fraction of currently allowed points are within the reach of these future experiments. Several of these currently allowed points also fall beneath the neutrino scattering floor shown in yellow, thus will remain outside the reach of any σ_{SI} -based future direct detection experiments.

The spin-independent DM-nucleon interaction is largely mediated through the t -channel ex-

change of CP-even Higgs bosons, where σ_{SI} can be expressed as [42],

$$\sigma_{SI} = \frac{4\mu_R}{\pi} |f|^2, \quad f \approx \sum_{i=1}^3 f_{H_i} = \sum_{i=1}^3 \frac{g_{H_i\tilde{\chi}_1^0\tilde{\chi}_1^0} g_{H_i NN}}{2m_{H_i}^2}, \quad (3.2)$$

where N denotes the nuclear states, μ_R is the reduced mass of the DM particle and the nucleon, and $g_{H_i\tilde{\chi}_1^0\tilde{\chi}_1^0}$ and $g_{H_i NN}$ denotes the coupling of the i^{th} CP-even Higgs bosons with the DM particle and the nucleons, respectively. For a Singlino-dominated $\tilde{\chi}_1^0$, characterized by $N_{15}^2 \sim 1$, the couplings with H_i are given by [60],

$$g_{H_i\tilde{\chi}_1^0\tilde{\chi}_1^0} \Big|_{\{\hat{h}, \hat{H}, \hat{s}\}} \approx \sqrt{2}\lambda [V_{H_i\hat{h}} N_{15} (N_{13} \sin \beta + N_{14} \cos \beta) + V_{H_i\hat{H}} N_{15} (N_{14} \sin \beta - N_{13} \cos \beta) + V_{H_i\hat{s}} (N_{13} N_{14} - \frac{\kappa}{\lambda} N_{15}^2)], \quad (3.3)$$

where we have retained N_{15} or $V_{H_i\hat{s}}$ dependent terms only. The Singlino-like $\tilde{\chi}_1^0$ couples with the CP-even Higgs bosons through its mixing with the Higgsinos. Additionally, it can couple with the singlet component on its own accord, with the coupling strength proportional to κ/λ , as indicated by Eq. (3.3).

The coupling of the i^{th} CP-even scalar with the nucleons is given by [84]

$$g_{H_i NN} \Big|_{\{\hat{h}, \hat{H}, \hat{s}\}} = \frac{m_N}{\sqrt{2}v} [V_{H_i\hat{h}} (F_d^{(N)} + F_u^{(N)}) + V_{H_i\hat{H}} (\tan \beta F_d^{(N)} - \frac{1}{\tan \beta} F_u^{(N)})] \quad (3.4)$$

where m_N denotes the mass of the nucleon and $F_{d,u}^{(N)}$ are the combined form factors associated with the atomic nuclear states. The coupling $g_{H_i NN}$ is primarily determined by the doublet-admixtures in the CP-even Higgs bosons and would be highly suppressed for a singlet-like Higgs boson.

Overall, for a Singlino-dominated $\tilde{\chi}_1^0$, a higher spin-independent DM-nucleon interaction rate is typically associated with greater Higgsino mixing, as suggested by Eqns. (3.3) and (3.4). To illustrate this, we show the amount of Higgsino admixture in the LSP $\tilde{\chi}_1^0$, $N_{13}^2 + N_{14}^2$, as a color palette in Fig. 2. It is observed that for higher DM masses, $m_{\tilde{\chi}_1^0} \gtrsim 100$ GeV, where consistency with the upper limit on relic density is achieved through co-annihilation (further discussed in Sec. 4), the parameter points excluded by the recent LZ limits are associated with a relatively larger Higgsino admixture. In contrast, in the lower $m_{\tilde{\chi}_1^0}$ regime, a large Higgsino admixture is not required for large σ_{SI} due to s -channel resonant annihilation mediated through a light Higgs boson.

It is important to note that there could be several conditions that result in a diminished value of σ_{SI} , falling below the neutrino floor. This could potentially arise from “blind spots” in the parameter space [60]. One such example is when coupling of SM-like Higgs with the Singlino-like $\tilde{\chi}_1^0$ s, $g_{H_{SM}\tilde{\chi}_1^0\tilde{\chi}_1^0}$, vanishes for either small λ or $m_{\tilde{\chi}_1^0}/\mu \simeq \sin 2\beta$ [46]. This SM-Higgs exchange process only applies when other CP-even Higgs bosons, H_s and H are decoupled and $H_s \gg H_{SM}$. Another important case related to our present study is the possibility of destructive interference from the CP-even singlet-like Higgs and the SM-like Higgs, $\sigma_{SI} \propto [V_{SM,\hat{h}} g_{H_{SM}\tilde{\chi}_1^0\tilde{\chi}_1^0}/m_{H_{SM}}^2 + V_{SM,\hat{s}} g_{H_s\tilde{\chi}_1^0\tilde{\chi}_1^0}/m_{H_s}^2]^2$. This is critical for $m_{H_s} < m_{H_{SM}}$ with the MSSM like Higgs boson, H being decoupled for both cases of Singlino-dominated LSP having large λ and small $\tan \beta$ and Higgsino-Singlino scenario. We refer the reader to Ref. [84] for further details. Also, it must be noted that a relatively light Bino/Wino-like state, characterized by

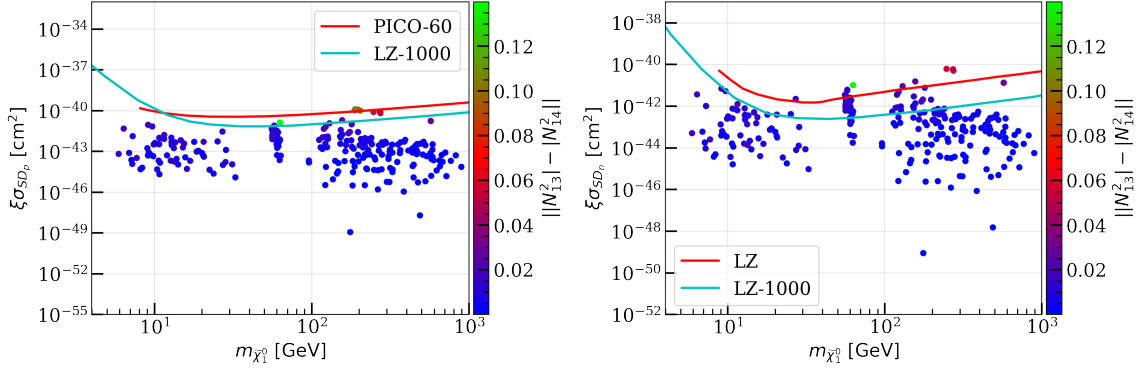


Figure 3: *Left:* The parameter space points allowed by the latest LZ SI limits in Fig.2 are plotted in the $\xi\sigma_{SD_p} - m_{\tilde{\chi}_1^0}$ plane. The red line represents the latest upper limit on σ_{SD_p} from PICO-60 [10]. *Right:* The allowed parameter points from the *Left* panel are plotted in the $\xi\sigma_{SD_n} - m_{\tilde{\chi}_1^0}$ plane. The current upper limit on σ_{SD_n} from LZ [9] are presented in red. The future sensitivity from LZ-1000 [11] on SD_p and SD_n is also projected in both panels. The color palette in both the panels represent the coupling $g_{Z\tilde{\chi}_1^0\tilde{\chi}_1^0} \propto N_{13}^2 - N_{14}^2$.

$m_{\tilde{\chi}_1^0} < M_1 < \mu < M_2$ or $m_{\tilde{\chi}_1^0} < M_1 < M_2 < \mu$, can induce gaugino-admixtures (gaugino is referred to Bino and Wino combinedly) in the Singlino-dominated LSP, which can potentially modify the usual blind spot condition for Z_3 symmetric NMSSM, revealing new parameter space for low σ_{SI} [35, 85].

The parameter space of interest can also be probed through spin-dependent DM-nucleon interactions. In this regard, we impose the most recent upper limits on the spin-dependent DM-neutron σ_{SD_n} and DM-proton σ_{SD_p} cross-sections from LZ [9] and PICO-60 [10], respectively, on the parameter points allowed by the previously discussed constraints, including the upper limits on $\xi\sigma_{SI}$. We show our results in Fig. 3. It is observed that only a few parameter space points are excluded by the upper limits on the spin-dependent interaction rate. Future projections for σ_{SD_n} and σ_{SD_p} for LZ-1000 [11] are also shown in the respective figures. The points allowed by the current upper limits on SD DM-neutron and DM-proton interactions will be henceforth referred to as the currently allowed parameter points.

The DM SD interactions are typically induced by t -channel exchange of Z boson. Their cross-section can be expressed as,

$$\sigma_{SD_{n/p}} \simeq C^{n/p} \times \left(\frac{g_{Z\tilde{\chi}_1^0\tilde{\chi}_1^0}}{0.01} \right)^2, \quad (3.5)$$

where n (p) denotes neutron (proton), with the nuclear form factor C^n (C^p) $\sim 10^{-41}$ cm², and the coupling $g_{Z\tilde{\chi}_1^0\tilde{\chi}_1^0}$ is determined by the Higgsino admixtures in the LSP $\tilde{\chi}_1^0$,

$$g_{Z\tilde{\chi}_1^0\tilde{\chi}_1^0} = \frac{m_Z}{\sqrt{2}v} (N_{13}^2 - N_{14}^2). \quad (3.6)$$

We illustrate the dependency of DM SD cross-sections on $||N_{13}|^2 - |N_{14}|^2||$ in Fig. 3 through the color palette. It is observed that the parameter points excluded by PICO-60 and LZ, through upper limits on σ_{SD-p} and σ_{SD-n} , respectively, are mostly in red, which corresponds to a relatively larger $||N_{13}|^2 - |N_{14}|^2||$. We would like to mention that all the allowed parameter points shown in Fig. 3 survive the constraints from DM indirect detection experiments [86], as shown in Appendix A.

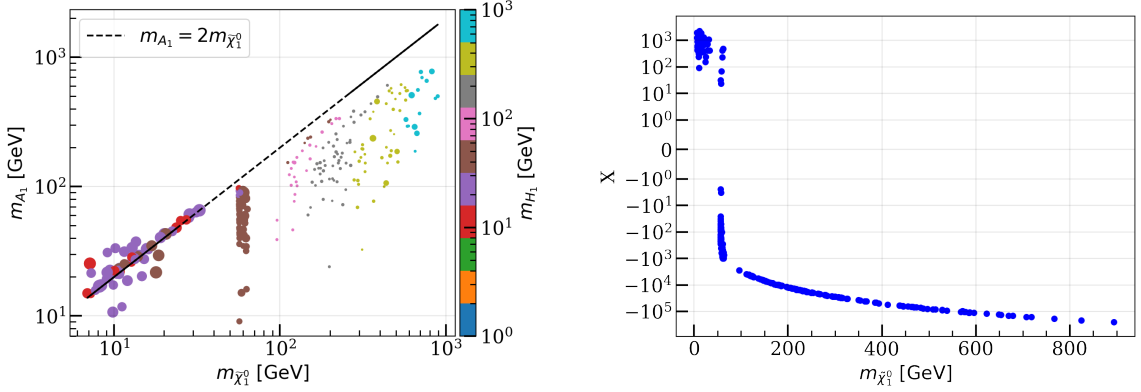


Figure 4: *Left:* The currently allowed parameter points are presented in the plane of $m_{\tilde{\chi}_1^0}$ and the mass of the singlet-dominated pseudoscalar Higgs boson A_1 . The color palette represents the mass of the singlet-dominated scalar Higgs boson H_1 . The diagonal black-dashed line corresponds to the condition: $m_{A_1} = 2m_{\tilde{\chi}_1^0}$. *Right:* The variation of X in Eq. (4.2) with the mass of the Singlino-dominated LSP $\tilde{\chi}_1^0$ is shown for the currently allowed parameter space points.

4 Annihilation processes with Singlino LSP

In this section, we examine the primary DM annihilation modes at different LSP masses. As discussed previously, our focus in this work is the region of parameter space where the LSP $\tilde{\chi}_1^0$ is Singlino-dominated, is consistent with the upper limit on the relic density $\Omega h^2 < 0.122$, and passes the relevant experimental constraints discussed in Sec. 3. The parameter space of interest contains points where the mass of the LSP spans from approximately 4 GeV to 1 TeV. Different DM annihilation modes ensure complicity with the relic density constraint at different LSP masses.

Within our parameter space of interest, the DM annihilation mechanisms include resonant s -channel annihilation via the exchange of singlet-like Higgs bosons A_1/H_1 , the Z boson, and the SM-like Higgs boson H_{SM} , t -channel annihilation via the exchange of a chargino or neutralino, and co-annihilation with the NLSP. For LSP masses below the Z -funnel, $m_{\tilde{\chi}_1^0} \lesssim m_Z/2$, it is observed that DM annihilation primarily proceeds via the s -channel exchange of a singlet-like Higgs boson A_1/H_1 with mass $m_{A_1/H_1} \sim 2m_{\tilde{\chi}_1^0}$. This is depicted in the left panel of Fig. 4, where we show the currently allowed parameter space points in the $m_{\tilde{\chi}_1^0}$ - m_{A_1} plane, with the z -axis representing m_{H_1} . The black-dashed line represents the condition $m_{A_1} = 2m_{\tilde{\chi}_1^0}$, indicating that a major fraction of points align with the criteria. For points in the lower LSP mass regime that are farther away from the $m_{A_1} = 2m_{\tilde{\chi}_1^0}$ line, it is observed that the lightest CP-even scalar H_1 is singlet-like, with mass $m_{H_1} \sim 2m_{\tilde{\chi}_1^0}$, indicating that DM annihilation proceeds through the exchange of resonant H_1 in the s -channel. Resonant annihilation predominantly proceeds via the exchange of the Z boson and the SM-like Higgs boson H_{SM} as we approach the Z and H_{SM} -funnel thresholds, corresponding to $m_{\tilde{\chi}_1^0} \sim m_Z/2$ and $m_{H_{SM}}/2$, respectively.

For the scenario involving a Singlino-like $\tilde{\chi}_1^0$ and the singlet-like Higgs bosons with negligible doublet-admixture, using Eqs. (2.7), (2.15) and (2.17), the mass-rule connecting the two can be

approximated as [35, 49],

$$\begin{aligned}\mathcal{M}_{\tilde{N},55}^2 &\equiv 4\kappa^2 v_S^2 = M_{S_R, S_R}^2 + \frac{1}{3}M_{S_I, S_I}^2 - \frac{4}{3}v_u v_d \left(\lambda^2 \frac{A_\lambda}{\mu} + \kappa \right) \\ &\approx \mathcal{M}_{S,33}^2 + \frac{1}{3}\mathcal{M}_{\mathcal{P},22}^2 - \frac{4}{3}v_u v_d \left(\lambda^2 \frac{A_\lambda}{\mu} + \kappa \right).\end{aligned}\quad (4.1)$$

Considering the singlet-like pseudoscalar Higgs mass twice the mass of the Singlino-like LSP $\tilde{\chi}_1^0$, $\mathcal{M}_{\mathcal{P},22}^2 = 4\mathcal{M}_{\tilde{N},55}^2 = 4m_{\tilde{\chi}_1^0}^2$, the condition necessary for resonant DM annihilation, Eq. (4.1) leads to,

$$\mathcal{M}_{S,33}^2 = -\frac{1}{3}m_{\tilde{\chi}_1^0}^2 + \frac{4}{3}v_u v_d \left(\lambda^2 \frac{A_\lambda}{\mu} + \kappa \right) \equiv X. \quad (4.2)$$

We illustrate the variation of X in Eq. (4.2) with the mass of Singlino-like LSP in the right panel of Fig. 4. Within the parameter space of our interest, X attains positive values only in the region $m_{\tilde{\chi}_1^0} \lesssim 50$ GeV. Eq. (4.2) and Fig. 4 (right) indicates that it is impossible to simultaneously achieve a physical mass for the singlet-like CP-even Higgs boson, $\mathcal{M}_{S,33}^2 > 0$, given $\mathcal{M}_{\mathcal{P},22}^2 \sim m_{A_1}^2 \geq 4\mathcal{M}_{\tilde{N},55}^2 \sim m_{\tilde{\chi}_1^0}^2$ for the Singlino-like $m_{\tilde{\chi}_1^0} \gtrsim 50$ GeV. This implies that within our parameter space, resonant DM annihilation through the exchange of a singlet-like Higgs boson in the s -channel is not viable for LSP masses above $\gtrsim 50$ GeV.

As indicated in Eq. (3.3), the coupling of the Singlino-dominated neutralinos with the singlet-dominated Higgs bosons relies on κ , which is typically smaller $\lesssim 0.1$ within our parameter space. Alternatively, it couples with the singlet-dominated Higgs bosons through its Higgsino admixture. At higher LSP masses, $m_{\tilde{\chi}_1^0} \gtrsim 100$ GeV, co-annihilation processes are required to comply with the relic density upper limits. This includes co-annihilation of Singlino-dominated LSP $\tilde{\chi}_1^0$ with the near-degenerate NLSP neutralino $\tilde{\chi}_2^0$ or chargino $\tilde{\chi}_1^\pm$ containing a non-trivial Higgsino admixture, $\text{LSP} + \text{NLSP} \rightarrow \text{SM}$ and the NLSP-NLSP ‘assisted’ co-annihilation, $\text{NLSP} + \text{NLSP} \rightarrow \text{SM}$. Typically, when $m_{\text{LSP}} \sim m_{\text{NLSP}}$, the thermal equilibrium between the LSP and the NLSP in the early universe can be maintained by the process $\text{LSP} + X \rightleftharpoons \text{NLSP} + X'$, where X and X' are SM fermions. This interaction is mediated via the t -channel exchange of gauge bosons or Higgs bosons, with interaction rates governed by $n_{\text{LSP}} n_X \langle \sigma v \rangle$, where n_{LSP} is the number density of the LSP and $\langle \sigma v \rangle$ represents the thermally-averaged cross-section times velocity [87]. The Higgsino admixture in the LSP $\tilde{\chi}_1^0$, although small but non-negligible, typically boosts these interactions within our parameter space of interest. Likewise, the rate of NLSP-NLSP annihilation process, $\text{NLSP} + \text{NLSP} \rightarrow \text{SM}$, scales as $\sim (n_{\text{NLSP}}^2 \langle \sigma v \rangle)$, where n_{NLSP} is the number density of the NLSPs. Near the freeze-out temperature, where the number density of SM fermions is several orders of magnitude larger than the NLSP, the interaction rate for the process $\text{LSP} + X \rightarrow \text{NLSP} + X'$ is typically larger than $\text{NLSP} + \text{NLSP} \rightarrow \text{SM}$. This allows the Singlino-dominated LSP $\tilde{\chi}_1^0$ to annihilate at a rate roughly comparable to that of the Higgsino-dominated NLSP, resulting in the observed under-abundant relic density. In the left panel of Fig. 5, we show the allowed parameter points in the $m_{\tilde{\chi}_1^0} - m_{\tilde{\chi}_1^\pm}$ plane. The red dashed line represents the mass degeneracy condition required for co-annihilation, $m_{\tilde{\chi}_1^0} = m_{\tilde{\chi}_1^\pm}$, and it is observed that the parameter points with $m_{\tilde{\chi}_1^0} \gtrsim 100$ GeV mostly lie along this line. In the z -axis, we show the minimum of the mass difference between the $\tilde{\chi}_1^0$ and $\tilde{\chi}_2^0/\tilde{\chi}_1^\pm$.

As discussed in Sec. 3, the chargino mass limits from LEP exclude Winos and Higgsinos up to 103.5 GeV [76]. The Higgsinos can be further constrained by direct searches at the LHC and direct detection experiments. However, within our parameter space of interest, due to mixing with the gauginos and depending on the relative values of M_1 and M_2 , the lower bounds on Higgsinos are

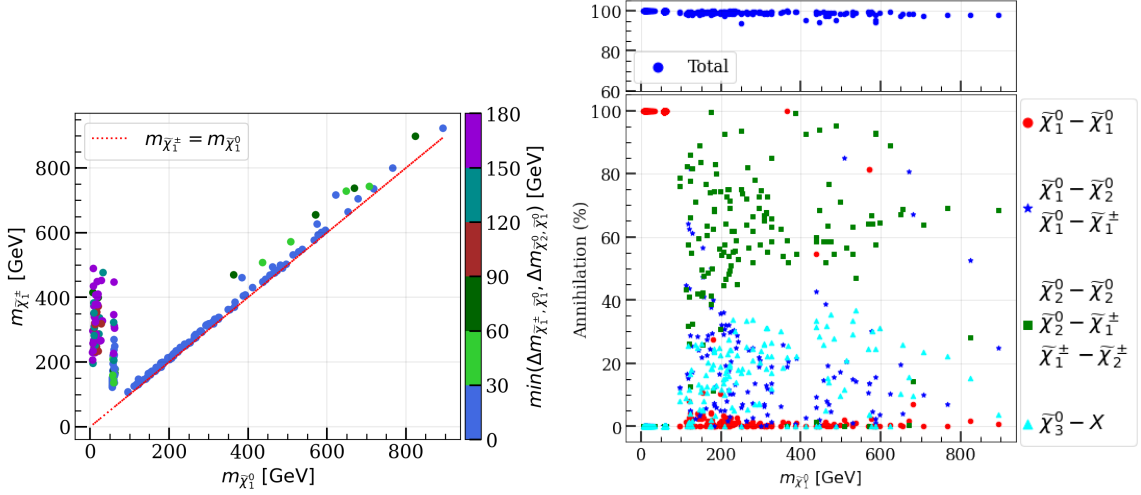


Figure 5: *Left:* Currently allowed parameter points are depicted in the $m_{\tilde{\chi}_1^\pm}$ versus $m_{\tilde{\chi}_1^0}$ plane. The z -axis represents the minimum of the mass difference between the Singlino-dominated $\tilde{\chi}_1^0$ and the NLSP $\tilde{\chi}_2^0/\tilde{\chi}_1^\pm$, $\min(\Delta m_{\tilde{\chi}_1^\pm, \tilde{\chi}_1^0}, \Delta m_{\tilde{\chi}_2^0, \tilde{\chi}_1^0})$. *Right:* The contribution percentage from the different DM annihilation modes in the early universe is shown for the allowed parameter points as a function of $m_{\tilde{\chi}_1^0}$. The points in red represent the contribution from $\tilde{\chi}_1^0 - \tilde{\chi}_1^0$ annihilation, including the resonant s -channel and t -channels. Contributions from co-annihilation with the $\tilde{\chi}_2^0$ or $\tilde{\chi}_1^\pm$ are shown in blue, while those from NLSP-NLSP-assisted co-annihilation are shown in green. The contribution from co-annihilation with the heavier neutralinos $\tilde{\chi}_3^0$ is depicted in sky-blue. The top panel represents the sum of contributions from the DM annihilation modes depicted in the lower panel.

significantly weakened. As a result, we obtain allowed points with Higgsino-dominated charginos and neutralinos as low as 110 GeV, with $m_{\tilde{\chi}_1^0}$ around the same mass, the criterion required for co-annihilation. It is worth noting that a sub-dominant contribution to the DM annihilation rate arises from $\tilde{\chi}_1^0 \tilde{\chi}_1^0$ annihilation into a pair of singlet-like light Higgs bosons: $\tilde{\chi}_1^0 \tilde{\chi}_1^0 \rightarrow H_1 H_1$ when $m_{\tilde{\chi}_1^0} > m_{H_1}$ and $m_{A_1} + m_{H_1} > 2m_{\tilde{\chi}_1^0}$, $\tilde{\chi}_1^0 \tilde{\chi}_1^0 \rightarrow A_1 A_1$ when $m_{\tilde{\chi}_1^0} > m_{A_1}$ and $m_{A_1} + m_{H_1} > 2m_{\tilde{\chi}_1^0}$, and $\tilde{\chi}_1^0 \tilde{\chi}_1^0 \rightarrow H_1 A_1$ when $m_{H_1} + m_{A_1} < 2m_{\tilde{\chi}_1^0}$. These annihilation channels can involve the s -channel exchange of the Z , H_1 , or A_1 bosons, or the t -channel exchange of $\tilde{\chi}_1^0$ and other heavier neutralinos.

We present the relative contribution (in %) from the different DM annihilation modes for our allowed parameter space points in the right panel of Fig. 5. The relative contribution from $\tilde{\chi}_1^0 - \tilde{\chi}_1^0$ annihilation in the s - or t -channels are shown in red, $\tilde{\chi}_1^0 - \tilde{\chi}_2^0/\tilde{\chi}_1^\pm$ co-annihilation is shown in blue, and NLSP-NLSP assisted co-annihilation is shown in green. The contribution from co-annihilation processes involving $\tilde{\chi}_3^0$ is shown in sky-blue. As discussed previously, resonant s -channel $\tilde{\chi}_1^0 - \tilde{\chi}_1^0$ annihilation is the dominant mode for DM dilution in the early universe for $m_{\tilde{\chi}_1^0} < m_{H_{SM}}/2$. At higher $\tilde{\chi}_1^0$ masses, co-annihilation with and assisted co-annihilation plays a crucial role in achieving consistency with the relic density limits.

5 Benchmark Scenario

Building on our understanding of the currently allowed parameter space, we now focus on examining the potential of probing these regions at the upcoming HL-LHC. One of the most promising modes

BPs	Parameters (GeV wherever applied)	Masses (GeV)	Cross-sections at 14 TeV (fb)	Interesting Processes & B.F.s(%)
BP	$\lambda = 0.174, \kappa = 0.007,$ $A_\lambda = 1384, A_\kappa = -70,$ $\tan\beta = 5.15, \mu = 229,$ $A_t = -6348, A_b = A_\tau = 2000,$ $A_\mu = 0, M_1 = 131.4,$ $M_2 = 965.8, M_3 = 3663,$ $N_{15} = 0.99, N_{21} = 0.95,$ $N_{23} = 0.26, N_{24} = 0.16,$ $N_{33} = N_{34} = 0.7,$ $N_{41}=0.3, N_{43} = N_{44} = 0.66$ $N_{52} = 0.99, \Gamma_{A_1} = 4.41 \times 10^{-5},$ $\Gamma_{H_1} = 9.47 \times 10^{-7}$	$m_{\tilde{\chi}_1^0} = 20.5, m_{\tilde{\chi}_2^0} = 123.9$ $m_{\tilde{\chi}_3^0} = 243, m_{\tilde{\chi}_4^0} = 244,$ $m_{\tilde{\chi}_5^0} = 1028, m_{\tilde{\chi}_1^\pm} = 233,$ $m_{\tilde{\chi}_2^\pm} = 1028, m_{H_1} = 14.2,$ $m_{H_2} = 125.1, m_{H_3} = 1169,$ $m_{H^\pm} = 1170, m_{A_1} = 43.8,$ $m_{A_2} = 1168$	$\tilde{\chi}_3^0 \tilde{\chi}_1^\pm = 194.4$ $\tilde{\chi}_1^\mp \tilde{\chi}_1^\pm = 116.4$ $\tilde{\chi}_4^0 \tilde{\chi}_1^\pm = 163.0$ $\tilde{\chi}_3^0 \tilde{\chi}_4^0 = 85.04$ $\tilde{\chi}_2^\pm \tilde{\chi}_1^\pm = 50.62$	$H_1 \rightarrow b\bar{b} = 82.4, H_1 \rightarrow \tau^+ \tau^- = 10.6,$ $H_3 \rightarrow \tilde{\chi}_2^0 \tilde{\chi}_3^0 = 13.8, A_2 \rightarrow \tilde{\chi}_2^0 \tilde{\chi}_4^0 = 12.0,$ $\tilde{\chi}_1^\pm \rightarrow \tilde{\chi}_1^0 W = 52.3, \tilde{\chi}_1^\pm \rightarrow \tilde{\chi}_2^0 W = 47.7,$ $\tilde{\chi}_2^\pm \rightarrow \tilde{\chi}_1^\pm Z = 25.6, \tilde{\chi}_2^\pm \rightarrow \tilde{\chi}_3^0 W = 24.8,$ $\tilde{\chi}_2^\pm \rightarrow \tilde{\chi}_1^\pm H_2 = 24.1, \tilde{\chi}_2^0 \rightarrow \tilde{\chi}_1^0 H_1 = 50.4,$ $\tilde{\chi}_2^0 \rightarrow \tilde{\chi}_1^0 Z = 46.3, \tilde{\chi}_3^0 \rightarrow \tilde{\chi}_1^0 Z = 31.4,$ $\tilde{\chi}_3^0 \rightarrow \tilde{\chi}_2^0 Z = 48.9, \tilde{\chi}_3^0 \rightarrow \tilde{\chi}_1^0 H_2 = 16.4,$ $\tilde{\chi}_4^0 \rightarrow \tilde{\chi}_1^0 Z = 45.3, \tilde{\chi}_4^0 \rightarrow \tilde{\chi}_2^0 Z = 14,$ $\tilde{\chi}_4^0 \rightarrow \tilde{\chi}_1^0 H_2 = 20.4, \tilde{\chi}_4^0 \rightarrow \tilde{\chi}_2^0 H_1 = 17.2,$ $\tilde{\chi}_5^0 \rightarrow \tilde{\chi}_3^0 Z = 21.4, \tilde{\chi}_5^0 \rightarrow \tilde{\chi}_1^\pm W = 50.4,$ $\tilde{\chi}_5^0 \rightarrow \tilde{\chi}_4^0 H_2 = 19.5$

Table 1: The input parameters, neutralino admixtures, masses and branching ratios of the electroweakinos and Higgs bosons, decay length of the light singlet-dominated Higgs bosons, and the cross-section of electroweakino pair production at $\sqrt{s} = 14$ TeV, for benchmark point BP.

to probe the electroweakinos at the LHC is through their direct production, as suggested by a plethora of studies such as [88–93]. However, our approach diverges from the traditional decay topologies, emphasizing NMSSM-specific scenarios aimed at exploring discovery prospects at the HL-LHC.

For our collider analysis, we examine a scenario from the allowed parameter region where the NLSP and LSP have non-degenerate masses, allowing the NLSP to decay promptly into the LSP. This configuration is observed in the low LSP mass regime, $m_{\tilde{\chi}_1^0} \lesssim m_Z/2$, where the primary DM dilution mode is characterized by resonant s -channel annihilation through a singlet Higgs boson with roughly twice the mass of the LSP. It is worth noting that in the co-annihilation regime with mass degenerate NLSP and LSP, the NLSPs may become long-lived, as previously explored in [44].

Within our parameter space of interest, featuring gaugino and Higgsino-dominated heavier

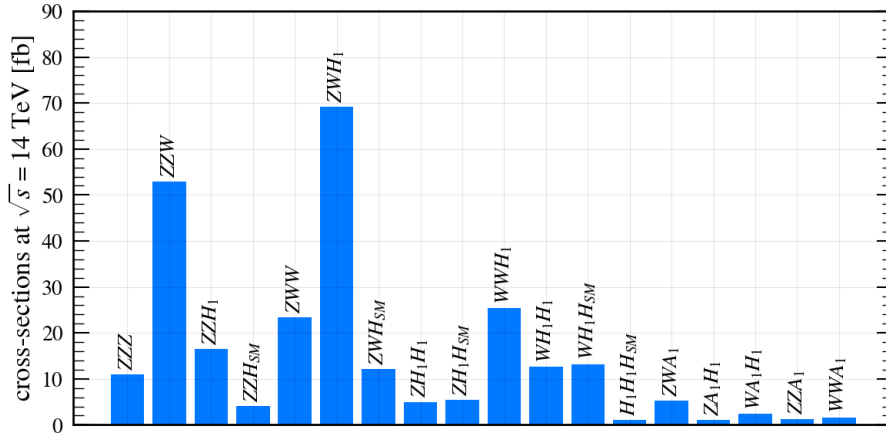


Figure 6: Production rates at the HL-LHC for all possible triple-boson channels from cascade decays of electroweakino pair production corresponding to benchmark point BP (see Table 1). Final states with a production rate of < 1 fb have been ignored.

neutralinos and charginos, appreciable pair production rates are expected at the LHC. With the Singlino-dominated state serving as the LSP DM, heavier electroweakino states will decay into it in a cascading manner, involving more steps compared to the MSSM scenario. The final state may also involve a light singlet-like Higgs boson, which is a characteristic feature in the NMSSM scenarios. The extended decay chain opens the possibility for probing these scenarios via final states involving triple-boson plus missing energy, $pp \rightarrow VVV + \cancel{E}_T$ ($V = Z, W^\pm, H_{SM}, H_1, A_1$), which can be challenging to achieve in the MSSM framework.

We consider a benchmark point BP from the low LSP mass regime, $m_{\tilde{\chi}_1^0} \lesssim m_{H_{SM}}/2$, in the allowed parameter space. The details of model parameters and the masses of electroweakinos and Higgs bosons are presented in Table 1. The branching ratios of the heavier charginos and neutralinos are also given, showing $\tilde{\chi}_2^0$ with mass $m_{\tilde{\chi}_2^0} = 123.9$ GeV as Bino-dominated with significant Higgsino admixture, while $\tilde{\chi}_3^0, \tilde{\chi}_4^0$ and $\tilde{\chi}_1^\pm$ being Higgsino-dominated with masses 243.2, 244.7 and 233.6 GeV, respectively. This configuration results in $\tilde{\chi}_1^\pm \tilde{\chi}_3^0 + \tilde{\chi}_1^\pm \tilde{\chi}_4^0$ having the highest production cross-section at the HL-LHC among all possible chargino-neutralino pair production channels. Alternatively, a benchmark point with a Higgsino-dominated NLSP $\tilde{\chi}_2^0$ could potentially lead to higher production rates for $\tilde{\chi}_1^\pm \tilde{\chi}_2^0$ and larger branching rates into final states with a singlet-like Higgs boson. However, it would preclude the triple-boson $+\cancel{E}_T$ final state. We proceed to analyze the production rates of potential triple-boson $+\cancel{E}_T$ final states arising from $pp \rightarrow \tilde{\chi}_1^\pm \tilde{\chi}_3^0 + \tilde{\chi}_1^\pm \tilde{\chi}_4^0$ for BP. We display our results in Fig. 6. Interestingly, the triple-boson final state with the highest production cross-section for BP is ZWH_1 , featuring a light singlet-dominated Higgs boson unique to NMSSM-specific scenarios. We consider this decay channel for our collider analysis in the next section.

6 Direct Electroweakino searches in the ZWH_1 channel

We perform a detailed collider analysis to probe the electroweakinos at the HL-LHC through searches in the $pp \rightarrow \tilde{\chi}_1^\pm \tilde{\chi}_3^0 + \tilde{\chi}_1^\pm \tilde{\chi}_4^0 \rightarrow ZWH_1 + \cancel{E}_T$ channel, considering the benchmark point BP. As highlighted in Sec. 6.1, we choose the ZWH_1 channel due to its higher production rate among all potential triple-boson final states arising from the cascade decay of directly produced $\tilde{\chi}_1^\pm \tilde{\chi}_3^0$ or $\tilde{\chi}_1^\pm \tilde{\chi}_4^0$ pairs. The cascade decay chain for the ZWH_1 channel is outlined as follows,

$$\begin{aligned} pp &\rightarrow \tilde{\chi}_1^\pm \tilde{\chi}_3^0 \rightarrow (\tilde{\chi}_1^\pm \rightarrow W^\pm \tilde{\chi}_1^0)(\tilde{\chi}_3^0 \rightarrow Z(\tilde{\chi}_2^0 \rightarrow H_1 \tilde{\chi}_1^0)) \rightarrow ZW^\pm H_1 + \cancel{E}_T, \\ &\rightarrow \tilde{\chi}_1^\pm \tilde{\chi}_4^0 \rightarrow (\tilde{\chi}_1^\pm \rightarrow W^\pm(\tilde{\chi}_2^0 \rightarrow H_1 \tilde{\chi}_1^0))(\tilde{\chi}_4^0 \rightarrow Z\tilde{\chi}_1^0) \rightarrow ZW^\pm H_1 + \cancel{E}_T. \end{aligned} \quad (6.1)$$

At benchmark point BP, the tree-level cross-section for the process $pp \rightarrow \tilde{\chi}_1^\pm \tilde{\chi}_3^0 + \tilde{\chi}_1^\pm \tilde{\chi}_4^0$ is approximately 358 fb at the $\sqrt{s} = 14$ TeV LHC, as detailed in Table 1. The cascade decay chain in Eq. 6.1 results in a production rate of approximately 43 fb for the ZWH_1 final state. For the analysis, we consider the dominant decay mode of H_1 : $H_1 \rightarrow b\bar{b}$, with a branching ratio of $Br(H_1 \rightarrow b\bar{b}) \sim 82.4\%$. Furthermore, we exclusively focus on the leptonic decay modes of the Z and W bosons due to their cleaner signatures at the detector and to avoid large QCD backgrounds. Thus, the signal process features a final state with three charged leptons, two bottom quarks, along with missing energy owing to the LSP $\tilde{\chi}_1^0$'s: $pp \rightarrow \tilde{\chi}_1^\pm \tilde{\chi}_3^0 + \tilde{\chi}_1^\pm \tilde{\chi}_4^0 \rightarrow ZW^\pm H_1 \rightarrow 3\ell + b\bar{b} + \cancel{E}_T$ ($\ell = e^\pm, \mu^\pm, \tau^\pm$). The leading order Feynman diagrams for the signal are presented in Fig. 7.

Dominant contributions to the background arise from top-pair production in association with the gauge bosons, $pp \rightarrow t\bar{t}W, t\bar{t}Z$, associated production with the SM Higgs boson, $t\bar{t}H_{SM}, ZWb\bar{b}$,

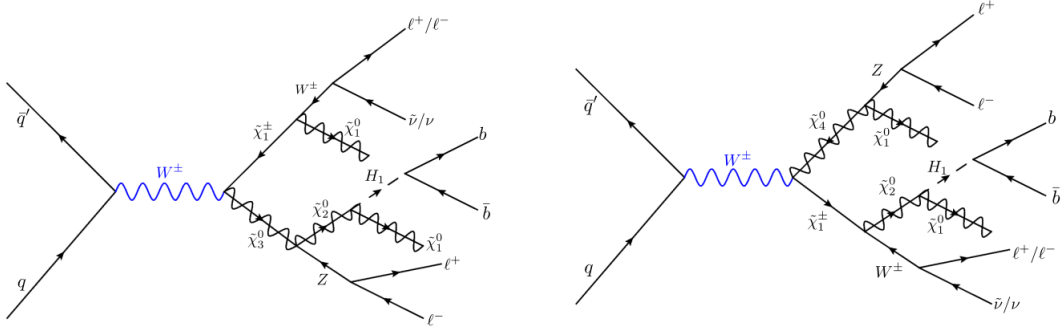


Figure 7: The leading order Feynman diagram for the signal process: $pp \rightarrow \tilde{\chi}_1^\pm \tilde{\chi}_3^0 + \tilde{\chi}_1^\pm \tilde{\chi}_4^0 \rightarrow ZW^\pm H_1 \rightarrow 3\ell + b\bar{b} + \cancel{E}_T$ ($\ell = e^\pm, \mu^\pm, \tau^\pm$).

VVV , VV +jets, and VH_{SM} processes, where $V = W^\pm, Z$. We consider all possible decay topologies in the background processes that lead to the $3\ell + b\bar{b} + \cancel{E}_T$ final state. Furthermore, sub-dominant contributions from tH_{SM} and $t\bar{t}VV$ processes are also included in the analysis.

The signal and background events are generated at the parton-level with **MG5aMC@NLO v2.9.16** [94] utilizing the **NNPDF23LO** parton distribution function [95] with the **A14** tune [96]. The signal events for BP are generated using the **NMSSM** model file [30, 97–99], with the masses, couplings, and branching ratios computed using **NMSSMTools**. Both signal and background events have been generated at the leading order, and higher-order effects are incorporated through K factors. Details of the generation-level cuts implemented in **MG5aMC@NLO v2.9.16** and cross-sections for the various processes have been included in Appendix B. Subsequently, showering and hadronization is performed using **Pythia-8** [100, 101], and fast detector response simulation is performed with **Delphes-3.5.0** [102], utilizing the default HL-LHC configuration card [103].

We select events containing exactly three isolated leptons l in the final state with transverse momentum $p_{T,\ell} \geq 15$ GeV and pseudorapidity $|\eta| < 4.0$. For electrons and muons, we impose the isolation criteria,

$$\frac{\sum p_T^{\Delta R < 0.2}}{p_{T,\ell'}} < 0.1 \quad \ell' = e, \mu, \quad (6.2)$$

where $\sum p_T^{\Delta R < 0.2}$ represents the sum of the transverse momentum of all other objects within a cone of radius $\Delta R \leq 0.2$ centred around the candidate lepton $\ell' = \{e, \mu\}$ carrying transverse momentum $p_{T,\ell'}$. Electrons and muons originating from the leptonically decaying τ 's are also subject to the isolation criteria in Eq. (6.2). For hadronically decaying tau leptons, τ_h , we apply tau-jet tagging efficiencies derived from CMS using the DeepTau algorithm [104]. These efficiencies are valid for τ_h with $p_{T,\tau_h} > 20$ GeV and within $|\eta| < 2.3$. In other kinematic regions, we adopt the default tau-jet tagging efficiencies provided in the HL-LHC configuration card. We also impose $p_{T,\ell_1} > 32$ GeV and $p_{T,\ell_2} > 20$ GeV, where ℓ_1 and ℓ_2 are the isolated leptons with the highest and 2nd highest transverse momentum, respectively. Furthermore, two of the isolated leptons are required to form a same flavor opposite sign (SFOS) lepton pair with invariant mass close to the mass of the Z boson, $|m_Z - m_{\ell\ell}^{SFOS}| < 15$ GeV. The basic event selection cuts discussed until this point are summarized in Table 2.

As discussed previously, a characteristic feature of our signal process is the presence of the

Basic selection cuts
$n_{\ell'} = 3$
$p_{T\ell_1, \ell_2, \ell_3} > 32, 20, 15 \text{ GeV}$
$ m_Z - m_{\ell\ell} < 15 \text{ GeV}$

Table 2: Summary of basic selection cuts.

light CP-even Higgs boson H_1 in the final state, which predominantly decays into a $b\bar{b}$ pair. For our benchmark point BP, H_1 with mass $m_{H_1} = 14.2 \text{ GeV}$ originates from the decay mode $\tilde{\chi}_2^0 \rightarrow H_1 \tilde{\chi}_1^0$, where $\tilde{\chi}_2^0$ and $\tilde{\chi}_1^0$ have masses of 123.9 and 20.5 GeV, respectively. The relatively lower mass of H_1 coupled with the considerable mass difference between $\{\tilde{\chi}_1^0 + H_1\}$ pair and the parent particle $\tilde{\chi}_2^0$, results in boosted H_1 , leading to collimated $b\bar{b}$ decay products which are typically challenging to resolve. The angular separation between the decay product of the light Higgs, $\Delta R_{b\bar{b}}$, depends on the Higgs mass m_{H_1} and its transverse momentum $p_T^{H_1}$ as approximated by $\Delta R_{b\bar{b}} \simeq m_{H_1}/(p_T^{H_1} \sqrt{z(1-z)})$ [105], where z and $1-z$ denote the fractions of momentum carried by the two decay products. Parton-level analysis shows a peak at $\Delta R_{b\bar{b}} \sim 0.2$, which reflects $p_{T,H_1} \gg m_{H_1}$. Given the relatively smaller $\Delta R_{b\bar{b}}$, we employ jet substructure techniques to identify the Higgs jet as a fatjet capable of capturing the inherent $b\bar{b}$ pair. We utilize the particle-flow (PF) algorithm [106, 107] to reconstruct fat-jets using e-flow objects in **Delphes** [102]. These e-flow objects are comprised of PF tracks, including charged particle tracks, and PF towers, including neutral particles and charged particles without any associated tracks, with corrected calorimeter smearings. The electrons and muons are separately included in the PF objects. These objects are given as input to the Cambridge-Aachen algorithm [108] with the jet radius parameter of $R = 0.7$ and the minimum p_T threshold of $> 40 \text{ GeV}$, implemented in the **FastJet v3.2.1** [109] setup. The fatjets within $|\eta| < 4.0$ are further groomed using the SoftDrop technique [110] with free parameters $\beta = 0$ and $z_{cut} = 0.1$, following standard CMS strategies [111]. To identify the soft-dropped fatjets as the light Higgs jets, we employ the Mass-drop tagger [105, 112] with parameters $\mu = 0.667$ and $y_{cut} > 0.01$, which identifies the two subjets j_a and j_b within the fatjets. j_a and j_b are then matched with the B -hadrons (the truth-level b -quarks just before hadronization) with $p_T > 10 \text{ GeV}$ and $|\eta| < 2.5$ at the generator-level, using a matching cone of radius $R < \min(0.3, \Delta R_{j_a, j_b}/2)$, where $\Delta R_{j_a, j_b}$ represents the separation between j_a and j_b . This choice is motivated from Ref. [105]. If both subjets satisfy these criteria, the fatjet is identified as a tagged light Higgs jet H^j . In events with more than one H^j , the one with invariant mass closest to m_{H_1} is associated with the light singlet-dominated Higgs boson H_1 . In this analysis, we impose the criteria, $n_{H^j} = 1$, where n_{H^j} is the number of tagged light Higgs fatjets. For our benchmark BP with $m_{H_1} = 14.2 \text{ GeV}$, the tagging efficiency of this method is roughly 20%. In the remainder of this analysis, we will refer to the tagged H_1 jet as H_1^j , while the two b -quark matched subjets within the H_1 jet will be referred to as b_1 and b_2 . In Fig. 8, we illustrate the mass distribution of the tagged Higgs jet, $m_{H_1^j}$, for the signal process $pp \rightarrow \tilde{\chi}_1^\pm \tilde{\chi}_3^0 \rightarrow ZW^\pm H_1 + \cancel{E}_T \rightarrow 3\ell + b\bar{b} + \cancel{E}_T$ (see Eq. (6.1)) and the dominant background processes. The $m_{H_1^j}$ distribution for the signal exhibits a sharp peak near m_{H_1} , owing to the comparatively smaller decay width of H_1 ($\Gamma_{H_1} = 9.47 \times 10^{-7} \text{ GeV}$), implying good mass resolution. On the other hand, the $m_{H_1^j}$ distributions for the background processes are flatter and do not exhibit any discernible sharp peaks. As such, the $m_{H_1^j}$ observable demonstrates an excellent potential for background reduction. We would like to note that a similar methodology

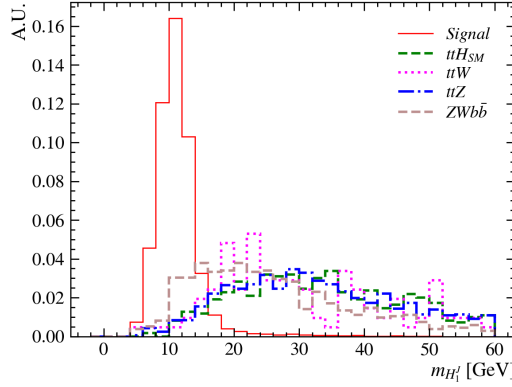


Figure 8: Distribution for the invariant mass of the tagged light Higgs jet H_1^j in the $pp \rightarrow \tilde{\chi}_1^\pm \tilde{\chi}_3^0 + \tilde{\chi}_1^\pm \tilde{\chi}_4^0 \rightarrow ZWH_1 + \cancel{E}_T \rightarrow 3\ell + b\bar{b} + \cancel{E}_T$ channel at the HL-LHC, corresponding to the benchmark point BP. Distributions for the dominant background processes are also illustrated.

can be extended to tau jets in scenarios where H_1 decays to $\tau_h \tau_h$ jets, offering further possibilities to improve the discovery potential of the signal at the LHC.

We perform a cut-based collider analysis by optimizing the selection cuts on

- $\Delta R(b_1, b_2)$: ΔR separation between the two b -like subjets associated with H_1^j ,
- \cancel{E}_T : missing transverse energy,
- $\Delta R(\ell_W, H_{1b_1b_2})$: ΔR separation between the non-SFOS lepton ℓ_W and $H_{1b_1b_2}$,
- $\Delta R(Z_{\ell\ell}^{SFOS}, H_{1b_1b_2})$: ΔR separation between the reconstructed Z boson and $H_{1b_1b_2}$,
- H_T : scalar sum of the transverse momentum of the three isolated leptons and the reconstructed H_1^j ,
- $m_{H_1^j}$: invariant mass of the reconstructed H_1 fatjet, and
- $M_T(H_1^j, \cancel{E}_T)$: transverse mass of the Higgs and missing energy system, defined as:

$$M_T(H_1^j, \cancel{E}_T) = \sqrt{m_{H_1^j}^2 + 2(E_T^{H_1^j} \cancel{E}_T - \vec{p}_T^{H_1^j} \cdot \vec{p}_T)}. \quad (6.3)$$

We tailor a signal region SR to maximize the signal significance σ_S for the signal process in Eq. (6.1) for the benchmark point BP (see Table 1). The signal significance σ_S is defined as,

$$\sigma_S = \frac{S}{\sqrt{B + (B * \delta_S)^2}}, \quad (6.4)$$

where S and B are the signal and background yields, respectively, and δ_S represents the systematic uncertainty.

We consider various combinations of selection cuts on the kinematic observables, aiming to maximize σ_S for the signal process. It is observed that the subset of observables $\{\cancel{E}_T, m_{H_1^j}, M_T(H_1^j, \cancel{E}_T)\}$ leads to the most optimal σ_S . In Fig. 9, we illustrate the \cancel{E}_T and $M_T(H_1^j, \cancel{E}_T)$ distributions for

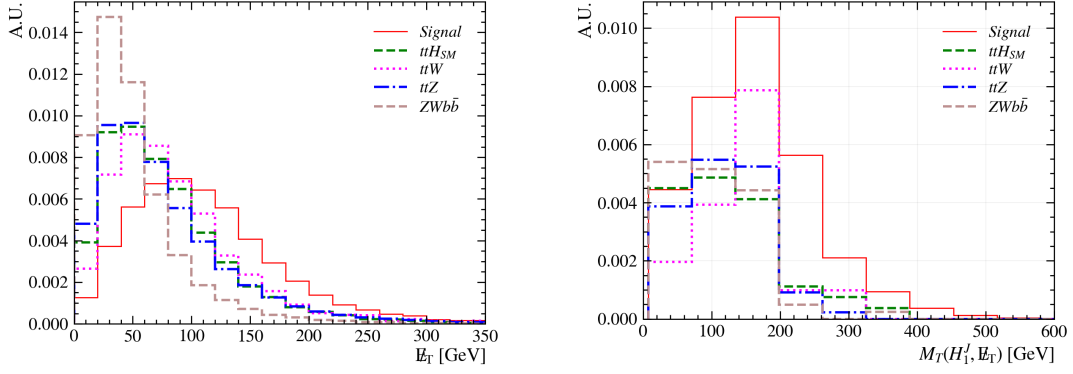


Figure 9: Distributions for the missing transverse energy E_T (*left*) and the transverse mass of the light Higgs fatjet and missing energy system $M_T(H_1^J, E_T)$ (*right*) in the $pp \rightarrow \tilde{\chi}_1^\pm \tilde{\chi}_3^0 + \tilde{\chi}_1^\pm \tilde{\chi}_4^0 \rightarrow ZWH_1 + E_T \rightarrow 3\ell + b\bar{b} + E_T$ channel at the HL-LHC, for benchmark point BP. Distributions for the dominant backgrounds are also shown.

the signal process and the dominant backgrounds: $t\bar{t}Z$, $t\bar{t}W$, $t\bar{t}H_{SM}$ and $ZWb\bar{b}$, after imposing the basic selection cuts in Table 2. The E_T distribution for the signal falls slowly compared to the backgrounds, with the tails extending to comparatively higher values. The $M_T(H_1^J, E_T)$ distribution for the signal displays a peak at $M_T(H_1^J, E_T) \sim 150$ GeV, while the background processes peak at smaller values. The optimized selection cuts, applied sequentially, are listed in Table 3, along with the signal and background yields at the $\sqrt{s} = 14$ TeV LHC with $\mathcal{L} = 3000 \text{ fb}^{-1}$. The event yields have been computed as $\sigma \times \text{BR} \times \epsilon \times \mathcal{L}$, where $\sigma \times \text{BR}$ are the production rates and ϵ is the efficiency defined as the ratio of the events that pass the cuts to the total number of events. The signal significance values, computed using Eq. (6.4), are also presented for hypothetical scenarios with null and 5% systematic uncertainties. We obtain a signal significance of $\lesssim 1$ upon the imposition of the basic selection cuts. At this stage, the signal over background ratio stands at roughly 10^{-4} . Imposing $n_{H^J} \geq 1$ and requiring the invariant mass of the H_1 fatjet to be less than 18 GeV resulted in $\sigma_S = 7.1$ and 6.7 for $\delta_S = 0$ and 5%, respectively, with $S/B \sim 1$. We further impose a minimum threshold on $M_T(H_1^J, E_T) > 150$ GeV, which improved σ_S to ~ 7.1 and 7.0, respectively. Our results indicate that the benchmark point BP can be probed at the HL-LHC through searches in the $pp \rightarrow ZW^\pm H_1 \rightarrow 3\ell + b\bar{b} + E_T$ channel with discovery potential ($\sigma_S > 5\sigma$).

Through this benchmark analysis, our goal is to emphasize the importance of conducting targeted searches specifically designed for the allowed parameter points. It is also worth noting that the search strategy employed in this analysis could impact other regions of the currently allowed parameter space, especially in the low $m_{\tilde{\chi}_1^0}$ regime where resonant s -channel annihilation plays a primary role in achieving the correct or underabundant DM relic density. Investigating the triple-boson final states involving H_1 or A_1 could be promising in these scenarios, and distinct signal regions could be designed for the parameter points featuring a light Higgs boson by adapting the cuts on the kinematic variables considered in these analyses. We intend to explore these aspects in future work.

	<i>SIG</i>	<i>ttW</i>	<i>ttZ</i>	<i>ttH_{SM}</i>	<i>ZWb\bar{b}</i>	<i>VVV</i>	<i>VV + jets</i>	<i>VH_{SM}</i>	<i>ttVV</i>	<i>tH_{SM}</i>	σ_s	
											$\delta_S = 0$	$\delta_S = 5\%$
$\sigma \times \text{BR} \times \ell$	2168	1207357	2009863	1173873	160243	903398	252096000	5368320	26438	169591	0.1	2×10^{-4}
Baseline Selection	402	2205	23181	5290	1136	5888	529371	14173	211	322	0.5	0.01
$E_T \geq 60$ GeV	317	1372	12082	2904	332	2521	121223	3029	138	93	0.8	0.04
$n_{H^\pm} = 1$	53	37	285	147	38	14	135	18	4	< 1	2.0	1.2
$m_{H^\pm} \leq 18$ GeV	51	4	24	11	8	0	0	0	0	0	7.1	6.7
$M_T(H_1^j, E_T) \geq 150$ GeV	26	2	7	3	1	0	0	0	0	0	7.1	7.0

Table 3: Signal and background yields in the $pp \rightarrow \tilde{\chi}_1^\pm \tilde{\chi}_3^0 + \tilde{\chi}_1^\pm \tilde{\chi}_4^0 \rightarrow ZWH_1 + E_T \rightarrow 3\ell + b\bar{b} + E_T$ channel at the HL-LHC. The yields are presented at each step of the cut-based analysis for the benchmark point BP and the background processes including $ttW, ttZ, ttH_{SM}, ZWb\bar{b}, VVV, VV + jets, VH_{SM}, ttVV$ and tH_{SM} . Signal significance at the HL-LHC is also presented for two scenarios: null and 5% systematic uncertainties.

7 Conclusion

In this work, we focused on exploring the parameter space within the NMSSM framework where a Singlino-dominated neutralino is a viable candidate for thermal dark matter. We concentrated on regions where the neutralino LSP's relic abundance is smaller than the observed cold dark matter relic density. The parameter space of our interest is constrained by various colliders and astrophysical probes, including LEP, rare B -meson decays, Higgs signal strengths, BSM Higgs searches, electroweakinos, sparticle searches at the LHC, and DM direct detection experiments. It is observed that a notable fraction of the currently allowed points are well within the reach of future spin-independent direct detection experiments. However, several currently allowed parameter points also lie below the neutrino scattering floor, rendering them inaccessible to future spin-independent direct detection probes.

In the low mass regime of the LSP neutralino, $m_{\tilde{\chi}_1^0} < m_Z/2$, resonant annihilation via the s -channel exchange of a light A_1 or H_1 with mass $\sim 2m_{\tilde{\chi}_1^0}$ is primarily responsible in achieving consistency with the upper limit on relic density. However, at higher LSP masses, $m_{\tilde{\chi}_1^0} \gtrsim m_{H_{SM}}/2$, the absence of an additional BSM Higgs boson at twice the LSP mass, as prohibited by the Higgs mass rule, restricts efficient DM dilution in the early universe through resonant annihilation via Higgs exchange. In this mass regime, consistency with the relic density constraints is achieved through co-annihilation with the NLSPs such as $\tilde{\chi}_2^0$ and $\tilde{\chi}_1^\pm$. Assisted co-annihilation, where the $\tilde{\chi}_1^0$ and the NLSP are in thermal equilibrium, also contributes significantly to DM annihilation before freeze-out.

Having identified the currently allowed parameter space, we then turned our attention to exploring non-conventional search channels to probe them at the HL-LHC. We particularly focus on identifying channels that would be rather challenging to access within the widely explored phenomenological-MSSM scenario. In this context, we explored the prospects of triple boson final states originating from direct electroweakino pair production in Sec. 5. We considered a benchmark point BP from the low LSP mass regime with $m_{\tilde{\chi}_1^0} = 20.5$ GeV from our allowed parameter space, featuring a light singlet-dominated pseudoscalar Higgs boson with twice the LSP mass and scalar Higgs boson at $m_{H_1} = 14.2$ GeV. We analyzed the production rates for all potential electroweakino pair-produced final states involving triple bosons. Our investigation revealed that the $ZWH_1 + E_T$

final state achieved the highest production rate for BP. This channel is particularly intriguing due to the presence of the light H_1 , making it specific to the NMSSM framework. We performed a detailed collider analysis in the $pp \rightarrow \tilde{\chi}_1^\pm \tilde{\chi}_3^0 + \tilde{\chi}_1^\pm \tilde{\chi}_4^0 \rightarrow ZW(H_1 \rightarrow b\bar{b}) + \cancel{E}_T \rightarrow 3\ell + b\bar{b} + \cancel{E}_T$ channel for BP in Sec. 6. Considering the boosted nature of H_1 , we perform a fatjet analysis and identify the two b -like subjets within the fatjets to effectively identify the Higgs jet. We have presented the details of the optimized selection cuts in Table 3 and obtained a signal significance of $\sim 7\sigma$, accounting for a systematic uncertainty of 5%. This illustrates the potential discovery capability of BP at the HL-LHC through searches in this channel.

Our results indicate the promising potential of performing benchmark-specific dedicated searches at the colliders to complement the conventional search strategies. It may be worth extending the search channel considered in this work to explore other allowed regions within our parameter space of interest. Furthermore, resonant heavy Higgs production decaying into the same electroweakino pairs could offer additional probes to further boost the sensitivity at the future colliders. We defer these explorations to a future work.

Acknowledgements

We would like to thank Aoife Bharucha for helpful discussions during the course of this work. A.A. received support from the French government under the France 2030 investment plan, as part of the Initiative d'Excellence d'Aix-Marseille Université - A*MIDEX. R.K.B.'s work is supported by World Premier International Research Center Initiative (WPI), MEXT, Japan.

A Indirect detection

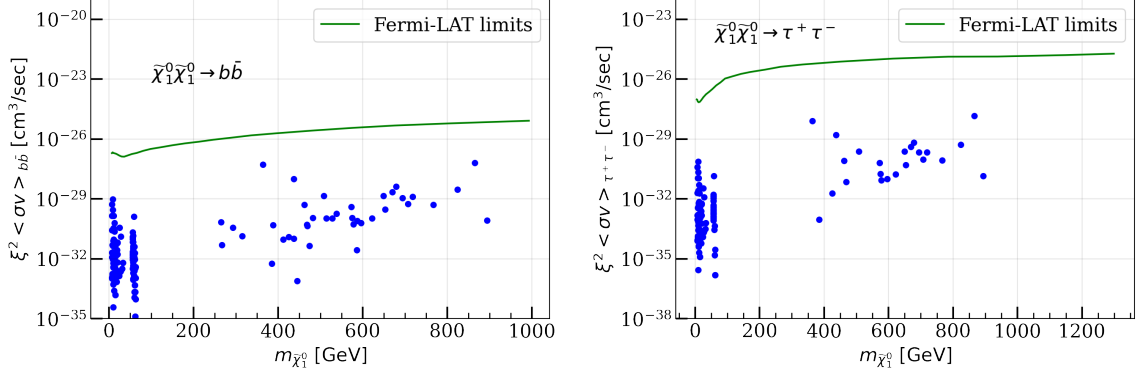


Figure 10: Allowed parameter space points are shown in the plane of ξ^2 scaled thermally averaged LSP DM annihilation cross section times velocity in the $b\bar{b}$ (left) and $\tau\tau$ (right) channels versus the LSP neutralino mass $m_{\tilde{\chi}_1^0}$.

B Summarising the cross sections and generator level cuts for the SM backgrounds

Backgrounds	Process	Generation-level cuts ($\ell = e^\pm, \mu^\pm, \tau^\pm$) (NA : Not Applied)	Cross section (fb)
$t\bar{t}Z$	$pp \rightarrow t\bar{t}Z$	NA	1046.9
$t\bar{t}W$	$pp \rightarrow t\bar{t}W^\pm$	NA	628.8
$t\bar{t}H_{SM}$	$pp \rightarrow t\bar{t}H_{SM}$	NA	611.4
$ZWb\bar{b}$	$pp \rightarrow ZW^\pm b\bar{b}$	$p_{T,b} > 15$ GeV, $ \eta_b < 4$, $\Delta R_{b,b} > 0.2$	83.46
VVV	$pp \rightarrow VVV, (V = W^\pm, Z)$	NA	470.5
VH_{SM}	$pp \rightarrow VH_{SM}$	NA	2796
$t\bar{t}VV$	$pp \rightarrow t\bar{t}VV$	NA	13.77
$t\bar{t}H_{SM}$	model loop SM $pp \rightarrow W^\pm \rightarrow H_{SM} \ t/\bar{t} \ b/\bar{b}$ [QCD]	$m_{\ell^+\ell^-} > 30$ GeV	3.18
	model loop SM no b mass $pp \rightarrow H_{SM} \ t/\bar{t} \ j \ j \ W^\pm$ [QCD]		85.15
$VV + jets$	$pp \rightarrow VVj$ $pp \rightarrow VVjj$	$p_{t,j} > 20$ GeV, $ \eta_j < 4$, $\Delta R_{j,j} > 0.2$	131300

Table 4: Generation level cuts and cross-sections for the various Standard Model backgrounds used in the analyses. Cross-sections are obtained from **Madgraph** LO value multiplied by the K factors.

References

- [1] Dan Hooper and Edward A. Baltz. Strategies for Determining the Nature of Dark Matter. *Ann. Rev. Nucl. Part. Sci.*, 58:293–314, 2008. [arXiv:0802.0702](https://arxiv.org/abs/0802.0702), [doi:10.1146/annurev.nucl.58.110707.171217](https://doi.org/10.1146/annurev.nucl.58.110707.171217).

- [2] Jonathan L. Feng. Dark Matter Candidates from Particle Physics and Methods of Detection. *Ann. Rev. Astron. Astrophys.*, 48:495–545, 2010. [arXiv:1003.0904](#), [doi:10.1146/annurev-astro-082708-101659](#).
- [3] Jessica Goodman, Masahiro Ibe, Arvind Rajaraman, William Shepherd, Tim M. P. Tait, and Hai-Bo Yu. Constraints on Light Majorana dark Matter from Colliders. *Phys. Lett. B*, 695:185–188, 2011. [arXiv:1005.1286](#), [doi:10.1016/j.physletb.2010.11.009](#).
- [4] Patrick J. Fox, Roni Harnik, Joachim Kopp, and Yuhsin Tsai. Missing Energy Signatures of Dark Matter at the LHC. *Phys. Rev. D*, 85:056011, 2012. [arXiv:1109.4398](#), [doi:10.1103/PhysRevD.85.056011](#).
- [5] N. Aghanim et al. Planck 2018 results. VI. Cosmological parameters. *Astron. Astrophys.*, 641:A6, 2020. [Erratum: *Astron. Astrophys.* 652, C4 (2021)]. [arXiv:1807.06209](#), [doi:10.1051/0004-6361/201833910](#).
- [6] Giorgio Arcadi, Máira Dutra, Pradipta Ghosh, Manfred Lindner, Yann Mambrini, Mathias Pierre, Stefano Profumo, and Farinaldo S. Queiroz. The waning of the WIMP? A review of models, searches, and constraints. *Eur. Phys. J. C*, 78(3):203, 2018. [arXiv:1703.07364](#), [doi:10.1140/epjc/s10052-018-5662-y](#).
- [7] Maira Dutra. *Origins for dark matter particles : from the "WIMP miracle" to the "FIMP wonder"*. PhD thesis, Orsay, LPT, 2019.
- [8] Manuel Drees, Hoernisa Iminniyaz, and Mitsuru Kakizaki. Constraints on the very early universe from thermal WIMP dark matter. *Phys. Rev. D*, 76:103524, 2007. [arXiv:0704.1590](#), [doi:10.1103/PhysRevD.76.103524](#).
- [9] J. Aalbers et al. First dark matter search results from the lux-zeplin (lz) experiment. *Phys. Rev. Lett.*, 131:041002, Jul 2023. URL: <https://link.aps.org/doi/10.1103/PhysRevLett.131.041002>, [doi:10.1103/PhysRevLett.131.041002](#).
- [10] C. Amole et al. Dark matter search results from the complete exposure of the pico-60 c3fs bubble chamber. *Phys. Rev. D*, 100:022001, Jul 2019. URL: <https://link.aps.org/doi/10.1103/PhysRevD.100.022001>, [doi:10.1103/PhysRevD.100.022001](#).
- [11] D. S. Akerib et al. Projected WIMP sensitivity of the LUX-ZEPLIN dark matter experiment. *Phys. Rev. D*, 101(5):052002, 2020. [arXiv:1802.06039](#), [doi:10.1103/PhysRevD.101.052002](#).
- [12] Junjie Cao, Lei Meng, Yuanfang Yue, Haijing Zhou, and Pengxuan Zhu. Suppressing the scattering of WIMP dark matter and nucleons in supersymmetric theories. *Phys. Rev. D*, 101(7):075003, 2020. [arXiv:1910.14317](#), [doi:10.1103/PhysRevD.101.075003](#).
- [13] Manuel Drees, Rohini Godbole, and Probir Roy. *Theory and Phenomenology of Sparticles*. WORLD SCIENTIFIC, 2005. URL: <https://www.worldscientific.com/doi/abs/10.1142/4001>, [arXiv:https://www.worldscientific.com/doi/pdf/10.1142/4001](#), [doi:10.1142/4001](#).
- [14] Howard Baer and Xerxes Tata. *Weak Scale Supersymmetry: From Superfields to Scattering Events*. Cambridge University Press, 2006. [doi:10.1017/CB09780511617270](#).
- [15] Lorenzo Calibbi, Jonas M. Lindert, Toshihiko Ota, and Yasutaka Takanishi. Cornering light Neutralino Dark Matter at the LHC. *JHEP*, 10:132, 2013. [arXiv:1307.4119](#), [doi:10.1007/JHEP10\(2013\)132](#).
- [16] Geneviève Bélanger, Guillaume Drieu La Rochelle, Béranger Dumont, Rohini M. Godbole, Sabine Kraml, and Suchita Kulkarni. LHC constraints on light neutralino dark matter in the MSSM. *Phys. Lett. B*, 726:773–780, 2013. [arXiv:1308.3735](#), [doi:10.1016/j.physletb.2013.09.059](#).

- [17] Rahool Kumar Barman, Genevieve Belanger, Biplob Bhattacharjee, Rohini Godbole, Gaurav Mendiratta, and Dipan Sengupta. Invisible decay of the Higgs boson in the context of a thermal and nonthermal relic in MSSM. *Phys. Rev. D*, 95(9):095018, 2017. [arXiv:1703.03838](#), [doi:10.1103/PhysRevD.95.095018](#).
- [18] M. Cahill-Rowley, J. L. Hewett, A. Ismail, and T. G. Rizzo. Lessons and prospects from the pMSSM after LHC Run I. *Phys. Rev. D*, 91(5):055002, 2015. [arXiv:1407.4130](#), [doi:10.1103/PhysRevD.91.055002](#).
- [19] Junjie Cao, Yangle He, Liangliang Shang, Wei Su, and Yang Zhang. Testing the light dark matter scenario of the MSSM at the LHC. *JHEP*, 03:207, 2016. [arXiv:1511.05386](#), [doi:10.1007/JHEP03\(2016\)207](#).
- [20] N. Arkani-Hamed, A. Delgado, and G. F. Giudice. The Well-tempered neutralino. *Nucl. Phys. B*, 741:108–130, 2006. [arXiv:hep-ph/0601041](#), [doi:10.1016/j.nuclphysb.2006.02.010](#).
- [21] Howard Baer, Vernon Barger, and Hasan Serce. SUSY under siege from direct and indirect WIMP detection experiments. *Phys. Rev. D*, 94(11):115019, 2016. [arXiv:1609.06735](#), [doi:10.1103/PhysRevD.94.115019](#).
- [22] Manimala Chakraborti, Utpal Chattopadhyay, and Sujoy Poddar. How light a higgsino or a wino dark matter can become in a compressed scenario of MSSM. *JHEP*, 09:064, 2017. [arXiv:1702.03954](#), [doi:10.1007/JHEP09\(2017\)064](#).
- [23] Peisi Huang, Roger A. Roglans, Daniel D. Spiegel, Yitian Sun, and Carlos E. M. Wagner. Constraints on Supersymmetric Dark Matter for Heavy Scalar Superpartners. *Phys. Rev. D*, 95(9):095021, 2017. [arXiv:1701.02737](#), [doi:10.1103/PhysRevD.95.095021](#).
- [24] Marcin Badziak, Marek Olechowski, and Pawel Szczerbiak. Is well-tempered neutralino in MSSM still alive after 2016 LUX results? *Phys. Lett. B*, 770:226–235, 2017. [arXiv:1701.05869](#), [doi:10.1016/j.physletb.2017.04.059](#).
- [25] Murat Abdughani, Lei Wu, and Jin Min Yang. Status and prospects of light bino–higgsino dark matter in natural SUSY. *Eur. Phys. J. C*, 78(1):4, 2018. [arXiv:1705.09164](#), [doi:10.1140/epjc/s10052-017-5485-2](#).
- [26] J. A. Casas, J. R. Espinosa, and I. Hidalgo. The MSSM fine tuning problem: A Way out. *JHEP*, 01:008, 2004. [arXiv:hep-ph/0310137](#), [doi:10.1088/1126-6708/2004/01/008](#).
- [27] Melissa van Beekveld, Sascha Caron, and Roberto Ruiz de Austri. The current status of fine-tuning in supersymmetry. *JHEP*, 01:147, 2020. [arXiv:1906.10706](#), [doi:10.1007/JHEP01\(2020\)147](#).
- [28] Ulrich Ellwanger, Gregory Espitalier-Noel, and Cyril Hugonie. Naturalness and Fine Tuning in the NMSSM: Implications of Early LHC Results. *JHEP*, 09:105, 2011. [arXiv:1107.2472](#), [doi:10.1007/JHEP09\(2011\)105](#).
- [29] Ulrich Ellwanger, Michel Rausch de Traubenberg, and Carlos A. Savoy. Particle spectrum in supersymmetric models with a gauge singlet. *Phys. Lett. B*, 315:331–337, 1993. [arXiv:hep-ph/9307322](#), [doi:10.1016/0370-2693\(93\)91621-S](#).
- [30] Ulrich Ellwanger, Cyril Hugonie, and Ana M. Teixeira. The Next-to-Minimal Supersymmetric Standard Model. *Phys. Rept.*, 496:1–77, 2010. [arXiv:0910.1785](#), [doi:10.1016/j.physrep.2010.07.001](#).
- [31] M. Maniatis. The Next-to-Minimal Supersymmetric extension of the Standard Model reviewed. *Int. J. Mod. Phys. A*, 25:3505–3602, 2010. [arXiv:0906.0777](#), [doi:10.1142/S0217751X10049827](#).

- [32] Jinrui Huang, Tao Liu, Lian-Tao Wang, and Felix Yu. Supersymmetric Exotic Decays of the 125 GeV Higgs Boson. *Phys. Rev. Lett.*, 112(22):221803, 2014. [arXiv:1309.6633](#), [doi:10.1103/PhysRevLett.112.221803](#).
- [33] Ulrich Ellwanger and Ana M. Teixeira. NMSSM with a singlino LSP: possible challenges for searches for supersymmetry at the LHC. *JHEP*, 10:113, 2014. [arXiv:1406.7221](#), [doi:10.1007/JHEP10\(2014\)113](#).
- [34] Sebastian Baum, Marcela Carena, Nausheen R. Shah, and Carlos E. M. Wagner. Higgs portals for thermal Dark Matter. EFT perspectives and the NMSSM. *JHEP*, 04:069, 2018. [arXiv:1712.09873](#), [doi:10.1007/JHEP04\(2018\)069](#).
- [35] Waleed Abdallah, Arindam Chatterjee, and Asesh Krishna Datta. Revisiting singlino dark matter of the natural Z_3 -symmetric NMSSM in the light of LHC. *JHEP*, 09:095, 2019. [arXiv:1907.06270](#), [doi:10.1007/JHEP09\(2019\)095](#).
- [36] Monoranjan Guchait and Arnab Roy. Light Singlino Dark Matter at the LHC. *Phys. Rev. D*, 102(7):075023, 2020. [arXiv:2005.05190](#), [doi:10.1103/PhysRevD.102.075023](#).
- [37] Ulrich Ellwanger, Cyril Hugonie, Stephen F. King, and Stefano Moretti. NMSSM Explanation for Excesses in the Search for Neutralinos and Charginos and a 95 GeV Higgs Boson. 4 2024. [arXiv:2404.19338](#).
- [38] Junjie Cao, Demin Li, Jingwei Lian, Yuanfang Yue, and Haijing Zhou. Singlino-dominated dark matter in general NMSSM. *JHEP*, 06:176, 2021. [arXiv:2102.05317](#), [doi:10.1007/JHEP06\(2021\)176](#).
- [39] Haijing Zhou, Junjie Cao, Jingwei Lian, and Di Zhang. Singlino-dominated dark matter in Z_3 -symmetric NMSSM. *Phys. Rev. D*, 104(1):015017, 2021. [arXiv:2102.05309](#), [doi:10.1103/PhysRevD.104.015017](#).
- [40] Sebastian Baum, Nausheen R. Shah, and Katherine Freese. The NMSSM is within Reach of the LHC: Mass Correlations & Decay Signatures. *JHEP*, 04:011, 2019. [arXiv:1901.02332](#), [doi:10.1007/JHEP04\(2019\)011](#).
- [41] Florian Domingo, Jong Soo Kim, Víctor Martín Lozano, Pablo Martín-Ramiro, and Roberto Ruiz de Austri. Confronting the neutralino and chargino sector of the NMSSM with the multilepton searches at the LHC. *Phys. Rev. D*, 101(7):075010, 2020. [arXiv:1812.05186](#), [doi:10.1103/PhysRevD.101.075010](#).
- [42] Junjie Cao, Yangle He, Liangliang Shang, Yang Zhang, and Pengxuan Zhu. Current status of a natural NMSSM in light of LHC 13 TeV data and XENON-1T results. *Phys. Rev. D*, 99(7):075020, 2019. [arXiv:1810.09143](#), [doi:10.1103/PhysRevD.99.075020](#).
- [43] Junjie Cao, Xinglong Jia, Lei Meng, Yuanfang Yue, and Di Zhang. Status of the singlino-dominated dark matter in general Next-to-Minimal Supersymmetric Standard Model. *JHEP*, 03:198, 2023. [arXiv:2210.08769](#), [doi:10.1007/JHEP03\(2023\)198](#).
- [44] Amit Adhikary, Rahool Kumar Barman, Biplob Bhattacharjee, Amandip De, Rohini M. Godbole, and Suchita Kulkarni. Long-lived NLSP in the NMSSM. *Phys. Rev. D*, 108(3):035020, 2023. [arXiv:2207.00600](#), [doi:10.1103/PhysRevD.108.035020](#).
- [45] Junjie Cao, Fei Li, Jingwei Lian, Yusi Pan, and Di Zhang. Impact of LHC probes of SUSY and recent measurement of $(g-2)$ on Z_3 -NMSSM. *Sci. China Phys. Mech. Astron.*, 65(9):291012, 2022. [arXiv:2204.04710](#), [doi:10.1007/s11433-022-1927-9](#).

- [46] Lei Meng, Junjie Cao, and Shenshen Yang. Dark Matter Physics in General NMSSM. 5 2024. [arXiv:2405.07036](#).
- [47] Qian-Fei Xiang, Xiao-Jun Bi, Peng-Fei Yin, and Zhao-Huan Yu. Searching for Singlino-Higgsino Dark Matter in the NMSSM. *Phys. Rev. D*, 94(5):055031, 2016. [arXiv:1606.02149](#), [doi:10.1103/PhysRevD.94.055031](#).
- [48] Ulrich Ellwanger. Present Status and Future Tests of the Higgsino-Singlino Sector in the NMSSM. *JHEP*, 02:051, 2017. [arXiv:1612.06574](#), [doi:10.1007/JHEP02\(2017\)051](#).
- [49] Ulrich Ellwanger and Cyril Hugonie. The higgsino-singlino sector of the NMSSM: combined constraints from dark matter and the LHC. *Eur. Phys. J. C*, 78(9):735, 2018. [arXiv:1806.09478](#), [doi:10.1140/epjc/s10052-018-6204-3](#).
- [50] Jong Soo Kim and Tirtha Sankar Ray. The higgsino-singlino world at the large hadron collider. *Eur. Phys. J. C*, 75:40, 2015. [arXiv:1405.3700](#), [doi:10.1140/epjc/s10052-015-3281-4](#).
- [51] Debottam Das, Ulrich Ellwanger, and Ana M. Teixeira. Modified Signals for Supersymmetry in the NMSSM with a Singlino-like LSP. *JHEP*, 04:067, 2012. [arXiv:1202.5244](#), [doi:10.1007/JHEP04\(2012\)067](#).
- [52] Georges Aad et al. Evidence for the production of three massive vector bosons with the ATLAS detector. *Phys. Lett. B*, 798:134913, 2019. [arXiv:1903.10415](#), [doi:10.1016/j.physletb.2019.134913](#).
- [53] G. Aad et al. Observation of WWW Production in pp Collisions at $\sqrt{s}=13$ TeV with the ATLAS Detector. *Phys. Rev. Lett.*, 129(6):061803, 2022. [arXiv:2201.13045](#), [doi:10.1103/PhysRevLett.129.061803](#).
- [54] Albert M Sirunyan et al. Observation of the Production of Three Massive Gauge Bosons at $\sqrt{s}=13$ TeV. *Phys. Rev. Lett.*, 125(15):151802, 2020. [arXiv:2006.11191](#), [doi:10.1103/PhysRevLett.125.151802](#).
- [55] Observation of heavy triboson production in leptonic final states in proton-proton collisions at $\sqrt{s}=13$ TeV. Technical report, CERN, Geneva, 2020. URL: <https://cds.cern.ch/record/2714899>.
- [56] David G. Cerdeño, Pradipta Ghosh, Chan Beom Park, and Miguel Peiró. Collider signatures of a light NMSSM pseudoscalar in neutralino decays in the light of LHC results. *JHEP*, 02:048, 2014. [arXiv:1307.7601](#), [doi:10.1007/JHEP02\(2014\)048](#).
- [57] Bhaskar Dutta, Yu Gao, and Bibhushan Shakya. Light Higgsino Decays as a Probe of the NMSSM. *Phys. Rev. D*, 91(3):035016, 2015. [arXiv:1412.2774](#), [doi:10.1103/PhysRevD.91.035016](#).
- [58] Florian Domingo. Decays of a NMSSM CP-odd Higgs in the low-mass region. *JHEP*, 03:052, 2017. [arXiv:1612.06538](#), [doi:10.1007/JHEP03\(2017\)052](#).
- [59] Ulrich Ellwanger and Stefano Moretti. Possible Explanation of the Electron Positron Anomaly at 17 MeV in ^8Be Transitions Through a Light Pseudoscalar. *JHEP*, 11:039, 2016. [arXiv:1609.01669](#), [doi:10.1007/JHEP11\(2016\)039](#).
- [60] Marcin Badziak, Marek Olechowski, and Paweł Szczerbiak. Blind spots for neutralino dark matter in the NMSSM. *JHEP*, 03:179, 2016. [arXiv:1512.02472](#), [doi:10.1007/JHEP03\(2016\)179](#).
- [61] D. J. Miller, R. Nevzorov, and P. M. Zerwas. The Higgs sector of the next-to-minimal supersymmetric standard model. *Nucl. Phys. B*, 681:3–30, 2004. [arXiv:hep-ph/0304049](#), [doi:10.1016/j.nuclphysb.2003.12.021](#).

- [62] Ulrich Ellwanger. Higgs Bosons in the Next-to-Minimal Supersymmetric Standard Model at the LHC. *Eur. Phys. J. C*, 71:1782, 2011. [arXiv:1108.0157](#), [doi:10.1140/epjc/s10052-011-1782-3](#).
- [63] Ulrich Ellwanger, John F. Gunion, and Cyril Hugonie. NMHDECAY: A Fortran code for the Higgs masses, couplings and decay widths in the NMSSM. *JHEP*, 02:066, 2005. [arXiv:hep-ph/0406215](#), [doi:10.1088/1126-6708/2005/02/066](#).
- [64] Ulrich Ellwanger and Cyril Hugonie. Nmhdecay 2.1: An updated program for sparticle masses, higgs masses, couplings and decay widths in the nmssm. *Computer Physics Communications*, 175(4):290–303, 2006. URL: <https://www.sciencedirect.com/science/article/pii/S0010465506001883>, [doi:https://doi.org/10.1016/j.cpc.2006.04.004](#).
- [65] Debottam Das, Ulrich Ellwanger, and Ana M. Teixeira. NMSDECAY: A Fortran Code for Supersymmetric Particle Decays in the Next-to-Minimal Supersymmetric Standard Model. *Comput. Phys. Commun.*, 183:774–779, 2012. [arXiv:1106.5633](#), [doi:10.1016/j.cpc.2011.11.021](#).
- [66] G. Belanger, F. Boudjema, A. Pukhov, and A. Semenov. MicrOMEGAs 2.0: A Program to calculate the relic density of dark matter in a generic model. *Comput. Phys. Commun.*, 176:367–382, 2007. [arXiv:hep-ph/0607059](#), [doi:10.1016/j.cpc.2006.11.008](#).
- [67] G. Belanger, F. Boudjema, A. Pukhov, and A. Semenov. Dark matter direct detection rate in a generic model with micrOMEGAs 2.2. *Comput. Phys. Commun.*, 180:747–767, 2009. [arXiv:0803.2360](#), [doi:10.1016/j.cpc.2008.11.019](#).
- [68] D. Barducci, G. Belanger, J. Bernon, F. Boudjema, J. Da Silva, S. Kraml, U. Laa, and A. Pukhov. Collider limits on new physics within micrOMEGAs 4.3. *Comput. Phys. Commun.*, 222:327–338, 2018. [arXiv:1606.03834](#), [doi:10.1016/j.cpc.2017.08.028](#).
- [69] Philip Bechtle, Sven Heinemeyer, Oscar Stål, Tim Stefaniak, and Georg Weiglein. *HiggsSignals*: Confronting arbitrary Higgs sectors with measurements at the Tevatron and the LHC. *Eur. Phys. J. C*, 74(2):2711, 2014. [arXiv:1305.1933](#), [doi:10.1140/epjc/s10052-013-2711-4](#).
- [70] Philip Bechtle, Sven Heinemeyer, Oscar Stål, Tim Stefaniak, and Georg Weiglein. Probing the Standard Model with Higgs signal rates from the Tevatron, the LHC and a future ILC. *JHEP*, 11:039, 2014. [arXiv:1403.1582](#), [doi:10.1007/JHEP11\(2014\)039](#).
- [71] Gaël Alguero, Jan Heisig, Charanjit K. Khosa, Sabine Kraml, Suchita Kulkarni, Andre Lessa, Humberto Reyes-González, Wolfgang Waltenberger, and Alicia Wongel. Constraining new physics with SModelS version 2. *JHEP*, 08:068, 2022. [arXiv:2112.00769](#), [doi:10.1007/JHEP08\(2022\)068](#).
- [72] Mohammad Mahdi Altakach, Sabine Kraml, Andre Lessa, Sahana Narasimha, Timothée Pascal, and Wolfgang Waltenberger. SModelS v2.3: Enabling global likelihood analyses. *SciPost Phys.*, 15(5):185, 2023. [arXiv:2306.17676](#), [doi:10.21468/SciPostPhys.15.5.185](#).
- [73] Philip Bechtle, Oliver Brein, Sven Heinemeyer, Georg Weiglein, and Karina E. Williams. HiggsBounds: Confronting Arbitrary Higgs Sectors with Exclusion Bounds from LEP and the Tevatron. *Comput. Phys. Commun.*, 181:138–167, 2010. [arXiv:0811.4169](#), [doi:10.1016/j.cpc.2009.09.003](#).
- [74] Philip Bechtle, Oliver Brein, Sven Heinemeyer, Georg Weiglein, and Karina E. Williams. HiggsBounds 2.0.0: Confronting Neutral and Charged Higgs Sector Predictions with Exclusion Bounds from LEP and the Tevatron. *Comput. Phys. Commun.*, 182:2605–2631, 2011. [arXiv:1102.1898](#), [doi:10.1016/j.cpc.2011.07.015](#).
- [75] Philip Bechtle, Oliver Brein, Sven Heinemeyer, Oscar Stål, Tim Stefaniak, Georg Weiglein, and Karina E. Williams. HiggsBounds – 4: Improved Tests of Extended Higgs Sectors against Exclusion

- Bounds from LEP, the Tevatron and the LHC. *Eur. Phys. J. C*, 74(3):2693, 2014. [arXiv:1311.0055](#), [doi:10.1140/epjc/s10052-013-2693-2](#).
- [76] G. Abbiendi et al. Search for chargino and neutralino production at $\sqrt{s}=192$ GeV to 209 GeV at LEP. *Eur. Phys. J. C*, 35:1–20, 2004. [arXiv:hep-ex/0401026](#), [doi:10.1140/epjc/s2004-01758-8](#).
- [77] Georges Aad et al. Observation of a new particle in the search for the Standard Model Higgs boson with the ATLAS detector at the LHC. *Phys. Lett. B*, 716:1–29, 2012. [arXiv:1207.7214](#), [doi:10.1016/j.physletb.2012.08.020](#).
- [78] Serguei Chatrchyan et al. Observation of a New Boson at a Mass of 125 GeV with the CMS Experiment at the LHC. *Phys. Lett. B*, 716:30–61, 2012. [arXiv:1207.7235](#), [doi:10.1016/j.physletb.2012.08.021](#).
- [79] Georges Aad et al. Combined Measurement of the Higgs Boson Mass in pp Collisions at $\sqrt{s} = 7$ and 8 TeV with the ATLAS and CMS Experiments. *Phys. Rev. Lett.*, 114:191803, 2015. [arXiv:1503.07589](#), [doi:10.1103/PhysRevLett.114.191803](#).
- [80] R. Agnese et al. Projected Sensitivity of the SuperCDMS SNOLAB experiment. *Phys. Rev. D*, 95(8):082002, 2017. [arXiv:1610.00006](#), [doi:10.1103/PhysRevD.95.082002](#).
- [81] Future dark matter searches with low-radioactivity argon. Input to the European Particle Physics Strategy Update 2018-2020 (2018). URL: https://indico.cern.ch/event/765096/contributions/3295671/attachments/1785196/2906164/DarkSide-Argo_ESPP_Dec_17_2017.pdf.
- [82] Marc Schumann, Laura Baudis, Lukas Büttikofer, Alexander Kish, and Marco Selvi. Dark matter sensitivity of multi-ton liquid xenon detectors. *JCAP*, 10:016, 2015. [arXiv:1506.08309](#), [doi:10.1088/1475-7516/2015/10/016](#).
- [83] J. Aalbers et al. DARWIN: towards the ultimate dark matter detector. *JCAP*, 11:017, 2016. [arXiv:1606.07001](#), [doi:10.1088/1475-7516/2016/11/017](#).
- [84] M. Badziak, M. Olechowski, and P. Szczerbiak. Blind spots for neutralinos in NMSSM with light singlet scalar. *PoS, PLANCK2015*:130, 2015. [arXiv:1601.00768](#).
- [85] Subhojit Roy and Carlos E. M. Wagner. Dark Matter searches with photons at the LHC. *JHEP*, 04:106, 2024. [arXiv:2401.08917](#), [doi:10.1007/JHEP04\(2024\)106](#).
- [86] A. Albert et al. Searching for Dark Matter Annihilation in Recently Discovered Milky Way Satellites with Fermi-LAT. *Astrophys. J.*, 834(2):110, 2017. [arXiv:1611.03184](#), [doi:10.3847/1538-4357/834/2/110](#).
- [87] A. Djouadi, U. Ellwanger, and A. M. Teixeira. Phenomenology of the constrained NMSSM. *JHEP*, 04:031, 2009. [arXiv:0811.2699](#), [doi:10.1088/1126-6708/2009/04/031](#).
- [88] Georges Aad et al. Search for direct production of charginos and neutralinos in events with three leptons and missing transverse momentum in $\sqrt{s} = 8$ TeV pp collisions with the ATLAS detector. *JHEP*, 04:169, 2014. [arXiv:1402.7029](#), [doi:10.1007/JHEP04\(2014\)169](#).
- [89] Morad Aaboud et al. Search for the direct production of charginos and neutralinos in final states with tau leptons in $\sqrt{s} = 13$ TeV pp collisions with the ATLAS detector. *Eur. Phys. J. C*, 78(2):154, 2018. [arXiv:1708.07875](#), [doi:10.1140/epjc/s10052-018-5583-9](#).
- [90] Georges Aad et al. Search for chargino-neutralino production with mass splittings near the electroweak scale in three-lepton final states in $\sqrt{s}=13$ TeV pp collisions with the ATLAS detector. *Phys. Rev. D*, 101(7):072001, 2020. [arXiv:1912.08479](#), [doi:10.1103/PhysRevD.101.072001](#).
- [91] Armen Tumasyan et al. Search for chargino-neutralino production in events with Higgs and W

- bosons using 137 fb^{-1} of proton-proton collisions at $\sqrt{s} = 13 \text{ TeV}$. *JHEP*, 10:045, 2021. [arXiv:2107.12553](#), [doi:10.1007/JHEP10\(2021\)045](#).
- [92] Armen Tumasyan et al. Search for electroweak production of charginos and neutralinos at $\sqrt{s}=13\text{TeV}$ in final states containing hadronic decays of WW, WZ, or WH and missing transverse momentum. *Phys. Lett. B*, 842:137460, 2023. [arXiv:2205.09597](#), [doi:10.1016/j.physletb.2022.137460](#).
 - [93] Georges Aad et al. Search for direct production of electroweakinos in final states with one lepton, jets and missing transverse momentum in pp collisions at $\sqrt{s} = 13 \text{ TeV}$ with the ATLAS detector. *JHEP*, 12:167, 2023. [arXiv:2310.08171](#), [doi:10.1007/JHEP12\(2023\)167](#).
 - [94] J. Alwall, R. Frederix, S. Frixione, V. Hirschi, F. Maltoni, O. Mattelaer, H. S. Shao, T. Stelzer, P. Torrielli, and M. Zaro. The automated computation of tree-level and next-to-leading order differential cross sections, and their matching to parton shower simulations. *JHEP*, 07:079, 2014. [arXiv:1405.0301](#), [doi:10.1007/JHEP07\(2014\)079](#).
 - [95] Richard D. Ball et al. Parton distributions for the LHC Run II. *JHEP*, 04:040, 2015. [arXiv:1410.8849](#), [doi:10.1007/JHEP04\(2015\)040](#).
 - [96] ATLAS Run 1 Pythia8 tunes. Technical Report ATL-PHYS-PUB-2014-021, CERN, Geneva, Nov 2014. URL: <http://cds.cern.ch/record/1966419>.
 - [97] A. Djouadi et al. Benchmark scenarios for the NMSSM. *JHEP*, 07:002, 2008. [arXiv:0801.4321](#), [doi:10.1088/1126-6708/2008/07/002](#).
 - [98] Peter Z. Skands et al. SUSY Les Houches accord: Interfacing SUSY spectrum calculators, decay packages, and event generators. *JHEP*, 07:036, 2004. [arXiv:hep-ph/0311223](#), [doi:10.1088/1126-6708/2004/07/036](#).
 - [99] B. C. Allanach et al. SUSY Les Houches Accord 2. *Comput. Phys. Commun.*, 180:8–25, 2009. [arXiv:0801.0045](#), [doi:10.1016/j.cpc.2008.08.004](#).
 - [100] Torbjorn Sjostrand, Stephen Mrenna, and Peter Z. Skands. PYTHIA 6.4 Physics and Manual. *JHEP*, 05:026, 2006. [arXiv:hep-ph/0603175](#), [doi:10.1088/1126-6708/2006/05/026](#).
 - [101] Torbjorn Sjostrand, Stephen Mrenna, and Peter Z. Skands. A Brief Introduction to PYTHIA 8.1. *Comput. Phys. Commun.*, 178:852–867, 2008. [arXiv:0710.3820](#), [doi:10.1016/j.cpc.2008.01.036](#).
 - [102] J. de Favereau, C. Delaere, P. Demin, A. Giammanco, V. Lemaître, A. Mertens, and M. Selvaggi. DELPHES 3, A modular framework for fast simulation of a generic collider experiment. *JHEP*, 02:057, 2014. [arXiv:1307.6346](#), [doi:10.1007/JHEP02\(2014\)057](#).
 - [103] Michele Selvaggi et al. Beta card for HL-LHC and HE-LHC studies, December 2017. https://github.com/delphes/delphes/blob/master/cards/delphes_card_HLLHC.tcl.
 - [104] Armen Tumasyan et al. Identification of hadronic tau lepton decays using a deep neural network. *JINST*, 17:P07023, 2022. [arXiv:2201.08458](#), [doi:10.1088/1748-0221/17/07/P07023](#).
 - [105] Jonathan M. Butterworth, Adam R. Davison, Mathieu Rubin, and Gavin P. Salam. Jet substructure as a new Higgs search channel at the LHC. *Phys. Rev. Lett.*, 100:242001, 2008. [arXiv:0802.2470](#), [doi:10.1103/PhysRevLett.100.242001](#).
 - [106] Morad Aaboud et al. Jet reconstruction and performance using particle flow with the ATLAS Detector. *Eur. Phys. J. C*, 77(7):466, 2017. [arXiv:1703.10485](#), [doi:10.1140/epjc/s10052-017-5031-2](#).
 - [107] Particle-Flow Event Reconstruction in CMS and Performance for Jets, Taus, and MET. 4 2009.

- [108] Yuri L. Dokshitzer, G. D. Leder, S. Moretti, and B. R. Webber. Better jet clustering algorithms. *JHEP*, 08:001, 1997. [arXiv:hep-ph/9707323](#), [doi:10.1088/1126-6708/1997/08/001](#).
- [109] Matteo Cacciari, Gavin P. Salam, and Gregory Soyez. FastJet User Manual. *Eur. Phys. J. C*, 72:1896, 2012. [arXiv:1111.6097](#), [doi:10.1140/epjc/s10052-012-1896-2](#).
- [110] Andrew J. Larkoski, Simone Marzani, Gregory Soyez, and Jesse Thaler. Soft Drop. *JHEP*, 05:146, 2014. [arXiv:1402.2657](#), [doi:10.1007/JHEP05\(2014\)146](#).
- [111] Albert M Sirunyan et al. Identification of heavy, energetic, hadronically decaying particles using machine-learning techniques. *JINST*, 15(06):P06005, 2020. [arXiv:2004.08262](#), [doi:10.1088/1748-0221/15/06/P06005](#).
- [112] Mrinal Dasgupta, Alessandro Fregoso, Simone Marzani, and Gavin P. Salam. Towards an understanding of jet substructure. *JHEP*, 09:029, 2013. [arXiv:1307.0007](#), [doi:10.1007/JHEP09\(2013\)029](#).